Drone-based large-scale particle image velocimetry applied to tidal stream energy resource assessment

Iain Fairley [a], *, Benjamin J. Williamson [b], Jason McIlvenny [b], Nicholas King [a], Ian Masters [a], Matthew Lewis [c], Simon Neill [c], David Glasby [a], Daniel Coles [d], Ben Powell [c], Keith Naylor [a], Max Robinson [a], Dominic E. Reeve [a]

[a] Faculty of Science and Engineering, Swansea University Bay Campus, Swansea, SA1 8EN, UK
[b] Environmental Research Institute, University of the Highlands and Islands, Thurso, KW14 7EE, UK
[c] School of Ocean Sciences, Bangor University, Menai Bridge, Anglesey, LL59 5AB, UK
[d] School of Engineering, Computing and Mathematics, University of Plymouth, Plymouth, Devon, PL4 8AA, UK

ARTICLE INFO

ABSTRACT

Resource quantification is vital in developing a tidal stream energy site but challenging in high energy areas. Drone-based large-scale particle image velocimetry (LSPIV) may provide a novel, low cost, low risk approach that improves spatial coverage compared to ADCP methods. For the first time, this study quantifies performance of the technique for tidal stream resource assessment, using three sites. Videos of the sea surface were captured while concurrent validation data were obtained (ADCP and surface drifters). Currents were estimated from the videos using LSPIV software. Variation in accuracy was attributed to wind, site geometry and current velocity. Root mean square errors (RMSEs) against drifters were 0.44 m s^{-1} for high winds (31 km/h) compared to 0.22 m s^{-1} for low winds (10 km/h). Better correlation was found for the more constrained site (r^2 increased by 4%); differences between flood and ebb indicate the importance of upstream bathymetry in generating trackable surface features. Accuracy is better for higher velocities. A power law current profile approximation enables translation of surface current to currents at depth with satisfactory performance (RMSE = 0.32 m s^{-1} under low winds). Overall, drone video derived surface velocities are suitably accurate for "first-order" tidal resource assessments under favourable environmental conditions.

1. Introduction

De-escalation of the climate crisis requires rapid decarbonisation of energy supplies in the pursuit of a net-zero future [1]. Tidal stream turbines are a promising form of predictable and sustainable low-carbon energy [2–4]; the devices convert kinetic energy from tidal flows and can be either mounted to the seabed or suspended from floating platforms. The global potential is large, with theoretical resources in coastal areas calculated at over 8000 TWh/yr [5]. Tidal energy is regular in cyclicity, easily predictable for years in advance [6,7] and of high quality [8] which means it has real potential to contribute to the future energy mix, with baseload possible through development of out-of-phase sites [9,10] or storage technology [6,11,12].

A key aspect of tidal stream project development is obtaining detailed information about flow characteristics at a site. This is vital for a range of purposes during the course of a project: at initial stages, knowledge of the basic resource is required to establish project viability, e.g. Refs. [13–22]; during the design stage, finer-scale understanding is required for array planning [23,24] and to microsite turbines [25,26]. Fine scale flow data are also required for environmental impact assessment and post-consent monitoring [27,28].

The standard approaches for measuring and understanding currents are acoustic Doppler current profiler (ADCP) campaigns, e.g. Refs. [29,30], validated numerical modelling, e.g. Ref. [14], or a

* Corresponding author.
E-mail addresses: i.a.fairley@swansea.ac.uk (I. Fairley), benjamin.williamson@uhi.ac.uk (B.J. Williamson), jason.mcilvenny@uhi.ac.uk (J. McIlvenny), nicholas.king@swansea.ac.uk (N. King), i.masters@swansea.ac.uk (I. Masters), m.j.lewis@bangor.ac.uk (M. Lewis), s.p.neill@bangor.ac.uk (S. Neill), david.glasby@swansea.ac.uk (D. Glasby), daniel.coles@plymouth.ac.uk (D. Coles), b.powell@bangor.ac.uk (B. Powell), k.naylor@swansea.ac.uk (K. Naylor), m.t.robinson@swansea.ac.uk (M. Robinson), d.e.reeve@swansea.ac.uk (D.E. Reeve).

combination of both, e.g. Ref. [21]. ADCP deployments provide high-accuracy measurements, but are limited in resolution: bed-mounted deployments provide good temporal resolution at one point [26], whereas vessel-mounted transects [29] provide better, though incomplete, spatial resolution but are limited temporally. Moreover, deployments can be costly and high risk. Additionally, with the development of floating tidal stream devices [31], interest in very near surface currents has increased. Establishing very near surface currents with standard ADCP deployment approaches [32] is difficult due to blanking distances and device mounting position [33]. Numerical modelling provides high spatial and temporal resolution data but requires calibration and validation against in-situ measurements: comparison against sparse point measurements, while the standard method, is not satisfactory for validation of highly spatio-temporally variable flows such as tidal stream sites [34].

These factors have led to interest in remote sensing to provide maps of surface currents at tidal stream sites; X-band and HF radar has been used for this purpose [35–40] but requires sufficient wave action to make measurements and significant land-based infrastructure. Satellites can also be used to map ocean flows but difficulties in measuring close to land and spatial resolution means they are not suited to tidal stream site characterisation [41,42]. Use of drones to derive high spatial resolution surface velocity maps of tidal stream sites has the potential to provide a complementary, low-cost, technique that may mitigate many of the above concerns. The technology would be particularly useful for first-pass screening of potential sites due to the portability of equipment and minimal financial burden, especially those sites in remote communities where standard resource assessment technology or vessels may not be available. The technique would also allow for real-world spatial measurements of turbine wake velocity deficit, which would be of great value to both the academic and industrial community.

Use of surface velocimetry to derive currents has become well established for fluvial applications where suitable accuracy can be achieved [43,44], and more recently drones have been used to collect the required video data [45,46]. Much less surface velocimetry work has been conducted in coastal or offshore environments and very little at tidal stream sites. Work that has been conducted in the nearshore environment includes surf-zone characterisation [47] and wave-induced current measurement [48–51]. Further offshore, both fixed video and drone-based surface velocimetry has been applied in large estuaries and tidal embayments [52,53]. However, at tidal stream energy sites, use of drones and surface velocimetry has focused on investigating the interaction between ecology and flow structure [54–56], rather than as a quantitative tool for resource assessment. To enable use of this technology for resource assessment, understanding of the accuracy and types of errors associated with the technique is required.

This study uses large-scale particle image velocimetry (LSPIV), the most common real-world surface velocimetry technique. Features are tracked between successive frames using cross-correlation of image subsections and hence velocity fields are derived [57]. Since laboratory-scale PIV makes use of seeding particles, some LSPIV studies have successfully used artificial tracers, e.g. Ref. [58], however there are practical and environmental constraints which prevents doing this at tidal stream sites. Instead, an unseeded approach will be used where the movement of ephemeral surface features such as foam patches or turbulent structures are tracked (sometimes called surface structure image velocimetry [59]). A range of open source tools are available for conducting PIV analysis, such as PIVlab [60,61], OpenPIV [62,63] or FUDAA-LSPIV [64]. In this paper, PIVlab is used; while PIVlab was originally developed for laboratory measurements, it has successfully been applied to real world flow monitoring in various settings, e.g. Refs. [65–72].

This study demonstrates the application of LSPIV to drone-collected video data of unseeded flows for the measurement surface currents at tidal stream sites and, for the first time, provides an accuracy assessment for these environments. This study focuses on results from Ramsey Sound in Pembrokeshire, Wales with supporting results from two other sites (Mumbles Head, Swansea, Wales and the Inner Sound of the Pentland Firth, Scotland) to demonstrate applicability to other locations.

2. Study sites

Three UK study sites are considered in this work: Mumbles Head, South Wales; Ramsey Sound, West Wales; and, the Inner Sound of the Pentland Firth, North Scotland (Fig. 1). The Inner Sound is an example of a more weather and wave exposed site compared to Ramsey Sound; while Mumbles Head is a shallow water environment.

2.1. Mumbles Head

Mumbles Head, South Wales (Fig. 1c) was used as an initial test site, and was included to provide analysis of method accuracy beyond "1st generation" tidal sites, where water depths are 20–50 m and mean spring peak currents exceed 2 m s^{-1} [73]. On the ebb phase of the tidal cycle, water exiting Swansea Bay is funnelled between two islands and current jets are generated on the southern side. Shallowest water depths were around 1.5 m during the experiment. The site is exposed to both swell and wind; during the experiment waves with a significant wave height of 0.7 m were present and highly visible in the video data (see example video A1 in appendix). Flights were undertaken from the beach at Bracelet Bay, directly to the west of the area of interest.

Supplementary video related to this article can be found at https://doi.org/10.1016/j.renene.2022.07.030

2.2. Ramsey Sound

Ramsey Sound is a channel between the Pembrokeshire coast and Ramsey Island (Fig. 1b); it runs north-south and is 3-km long with widths between 0.7 and 1.6 km. There has been significant interest in tidal stream energy extraction at the location, with Tidal Energy Ltd.'s DeltaStream device being deployed in 2015 [74] and the site being currently re-developed by Cambrian Offshore [75]. Therefore, there has been substantial research into the characteristics of tidal dynamics in the sound [29,37,76–78]. Currents in the region are forced by a progressive tidal wave and so are at a maximum around high (flood tide) and low water (ebb tide). Flood tide currents are directed northward and ebb tide currents are directed southward. The site is well protected from waves from the prevailing south westerly direction, although exposed to waves incident from the north.

Flights were conducted from land over the north-eastern part of the sound (Fig. 1b), close to the DeltaStream deployment site but further east due to flight distance limit regulations of 500 m from the operator. This means that on the flood tide, water has travelled through the sound, including the highly irregular bathymetry of 'The Bitches' and 'Horse Rock,' before reaching the study area; whereas on the ebb tide water is travelling into the sound from the more uniform offshore area (Fig. 2). Thus, one might expect greater turbulent features to be present on the flood tide compared to the ebb; ADCP analysis has previously shown that flood tides have greater turbulent kinetic energy than ebb tides at the DeltaStream site [26].
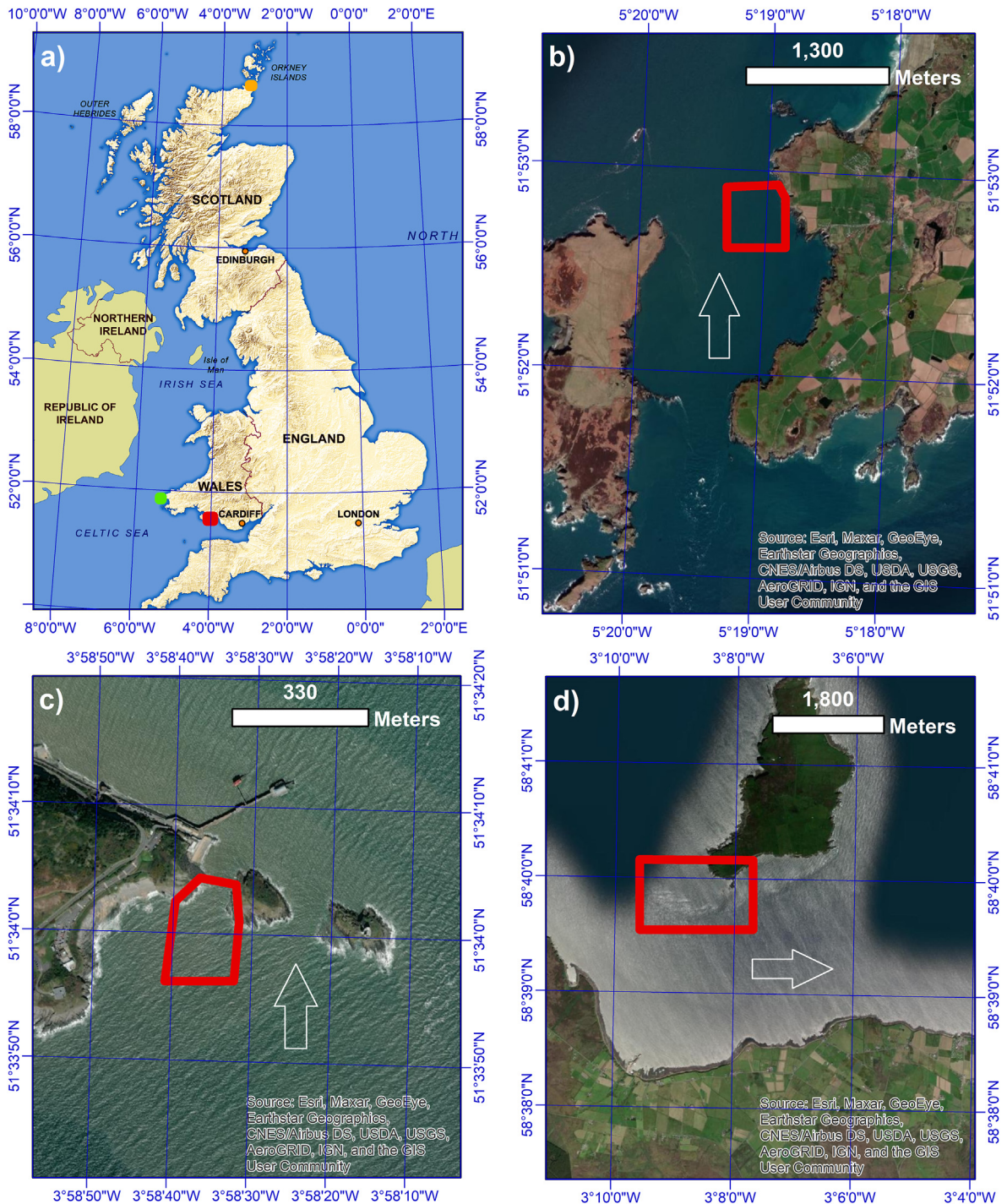
Fig. 1. a) Location of the three study sites (Mumbles Head in red, Ramsey Sound in green, Pentland Firth in orange); and, aerial imagery for b) Ramsey Sound; c) Mumbles Head; d) Inner Sound of the Pentland Firth. Indicative flight areas are shown as red polygons. White outline arrows indicate the direction of flood tide currents.

2.3. Inner Sound of the Pentland Firth

The Inner Sound of the Pentland Firth (Fig. 1d) is one of the most well-known locations for tidal stream energy, being host to the MeyGen project [80]. The Pentland Firth is the body of water between the north coast of the Scottish mainland and the Orkney Islands. The island of Stroma is situated in the Firth and the channel between it and mainland is known as the Inner Sound. There has been extensive research in this area and a range of measured and modelled current assessments, e.g. Refs. [30,81–83]. There is a 2-hr phase difference in the M_2 tidal wave between the eastern and western approaches of the Pentland Firth which causes a hydraulic gradient that forces currents greater than 5 m s^{-1} [83]. In the Inner Sound, current flows are complex, with strong asymmetry and misalignment; currents can reach 4 m s^{-1} [30]. The Inner Sound runs approximately west – east with widths of 2.5–3 km and a length of ~6 km (approximately double the size of Ramsey Sound). As well as being larger than Ramsey Sound, it is less constrained by
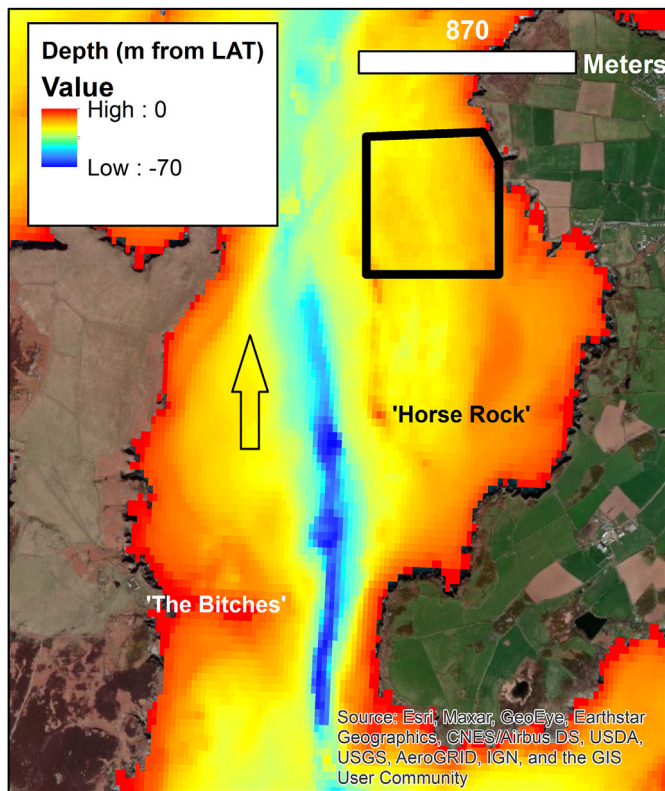
Fig. 2. The Bathymetry of Ramsey Sound with key features labels and the flight area indicated as a black polygon. The black outline arrow indicates direction of the flood tide. Bathymetry [79] © British Crown and OceanWise, 2021. All rights reserved. Licence No. EK001-20180802. Not to be used for Navigation.

the bounding coastlines. The site is more exposed to wind and waves than Ramsey Sound, both due to the site scale and due to regional wave climate being more energetic.

A flight was conducted from a boat at the western end of the Inner Sound, close to the island of Stroma. One characteristic of the Inner Sound is the presence of kolk boils, which are surface manifestation of turbulence advected from the seabed and can be seen in drone imagery as very smooth regions [56]. These are common at a range of tidal sites, were present in the collected imagery (see video A5 in appendix) and may lead to regions with minimal tracers for PIV analysis.

3. Methodology

The basic concept of this approach is to hover a drone over an area of interest and collect video data which can subsequently be analysed with PIVlab to obtain surface velocimetry measurements. Concurrent validation data are collected to assess technique performance. As well as PIV tests, stability tests for the drone platform were conducted to establish the magnitude of errors relating to station-keeping and positioning.

3.1. Flight methodology

Table 1 provides a summary of flights, conditions and validation data collected (validation data covered in section 3.2). The experiment at Mumbles Head was conducted for 1 h starting 1.25 h after high water; during that time the water level dropped by 1.53m from 8.92m to 7.39m. At Ramsey Sound, data was collected through both the flood and ebb phases of the tide on the 12th and just for

the flood tide on the 14th. Fig. 3 shows a timeseries of tidal elevation and velocity magnitude, output from a numerical model of the area [37], with times of analysed videos and ADCP datapoints overlain; slightly different strategies were employed on each day meaning that there was less temporal separation between ADCP and video on the 14th. At the Pentland Firth, one flight was conducted, 1 h before high tide. Example video data from each of the sites is given as embedded videos in Appendix A; this shows the range of surface conditions that were covered.

Two different drone and camera combinations were used in this study. At Mumbles Head and Ramsey Sound, data were obtained using a Zenmuse X7 camera with a 35 mm lens mounted on a DJI M210 v2 RTK drone (hereafter referred to as M210). At Mumbles Head, the drone was flown with standard GPS and at Ramsey Sound in RTK GPS mode with the DJI base station. For the flight at the Inner Sound of the Pentland Firth, a DJI Phantom 4 Pro 2.0 drone with built-in camera was used (hereafter referred to as Phantom). This drone operates using standard GPS and was included to demonstrate capability using lower-cost 'consumer-grade' drones.

The drones were flown manually to the areas of interest and hovered at 120 m above surface while collecting nadir (downward facing) video imagery. 120 m is the maximum height permissible for drone flights in the UK and was used to ensure the largest field of view; for the cameras used, this is 66 m × 117.5 m (M210) and 109.1 m × 206.8 m (Phantom). Video frames from the M210 had dimensions of 2160 x 3824 pixels (px), whereas frames from the Phantom had dimensions 2160 x 2096 px. In both cases the video was acquired at 30 frames per second (fps). Nadir imagery was collected to facilitate georeferencing without ground control points; ground control is unlikely to be available at many tidal stream sites.

Video data were collected by the M210 in DJI 'dewarp' mode, meaning that lens distortion was removed automatically; for the Phantom, this facility did not exist, and no correction was applied. It has previously been demonstrated that ignoring lens distortion does not induce significant errors for drone-based video [84]. For cases where lens distortion is considered critical, and where internal dewarping procedures are not available, lens distortion can easily be calculated and removed, e.g. Ref. [85]. The gimbal was set to 'free' mode, such that it maintains its orientation independent of drone movement.

Georeferencing can then be conducted based on GPS position information, drone altitude and gimbal heading information, similar to approaches used previously [53,84]. Nadir imagery means rectification of the imagery is not required and the drone x,y position is equal to the x,y, position of the centre of the image. The gimbal heading is used to orientate the y axis of the image. The ground sampling distance, the length of one pixel at sea level, can then be used to assign real world coordinates to all pixels. Ground sampling distance (GSD) (in metres) can be calculated based on the height above surface and camera parameters using:

$$GSD = \frac{S_w \times H}{F_r \times I_w}$$

where S_w is the sensor width in mm, H is the flight height above surface in metres, F_r is the focal length of the camera in mm and I_w is the image width in pixels. The height above surface was calculated using the altitude above take-off in the flight log and the elevation difference between water level and take off level. For the initial tests at Mumbles Head, the drone was flown from the beach and take-off level was approximately the water level. At Ramsey Sound, tidal elevation data at two nearby UK National Tidal and Sea Level Facility gauges (Milford Haven to the south and Fishguard to the north) was used to estimate water levels in Ramsey Sound for

Table 1
A summary of the conditions and validation data collected during fieldwork.

| Date	Site	Drone	No. videos analysed	Tide state	Wind Speed (km/h)	Environmental conditions	Validation data
02/03/2021	Mumbles Head	M210	7	ebbing	20	Overcast, 0.7 m waves	Drifter
12/05/2021	Ramsey Sound	M210 with RTK	11	Flood and ebb	31	Overcast	Drifter and ADCP (ADCP flood only)
14/05/2021	Ramsey Sound	M210 with RTK	11	Flood	10	Bright sunshine	Drifter and ADCP
02/07/21	Inner Sound	Phantom	1	Flood	16	Overcast	ADCP
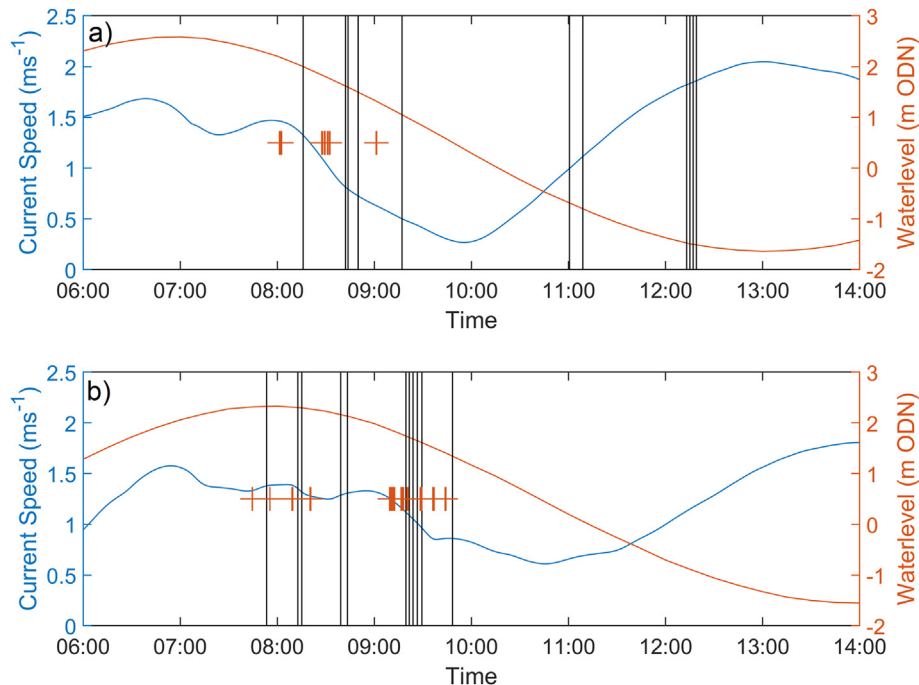
Fig. 3. Hydrodynamic timeseries describing the experiments at Ramsey Sound for: a) 12th May, and b) 14th May. The blue lines give current speed and the orange lines tidal elevation. On top of these, the vertical black lines indicate times of analysed video segments and the orange crosses times of ADCP measurements. The drifters, which were measuring more frequently, are not shown.

the various flights. The Phantom was flown from a vessel in the Inner Sound and altitude above sea level taken from the flight log. Mean values from the flight logs were calculated for all video segments and it was assumed the drone remained completely stationary during each 1 min video recording.

To validate this approach, stability of drone hovering and the accuracy of the georectification procedure were tested with land-based experiments using the M210 for a range of windspeeds. A grid of black and white lino tiles were arranged on a flat grass field and their positions surveyed using a TopCon HiPerV network RTK GPS with accuracy of approximately 0.01 m; the target in the centre was made up of four tiles to stand out (Fig. 4). Two-dimensional cross correlation of a template covering the central target was used to assess frame on frame stability of the drone hover. For this aspect, wind speeds at the drone were taken from the in-flight wind readings of AirdataUAV; in-flight wind is calculated based on motor readings, drone speed, IMU data and aerodynamic profile of the drone. Accuracy of the georectification was tested by manually identifying targets in the geo-referenced image and comparing to the surveyed positions.

3.2. Validation data collection

Validation data were collected both with surface drifters (Mumbles Head and Ramsey Sound) and use of the uppermost bin of ADCP transects (Ramsey Sound and Inner Sound). Mumbles Head

was too shallow to allow for ADCP transects, and environmental conditions during the Inner Sound fieldwork meant drifters would not have been successfully recovered.

Four low-cost surface drifters were constructed based on a Davis drifter design [86], see Fig. 5. Drifter frames were made from PVC pipe and plumbing fittings, with tarpaulin stretched between the frame to act as the sails. Buoyancy was provided by sections of foam attached to the top arms of the frame and stability provided by 0.17 kg fishing weights attached to each lower arm. The sails captured the top 0.5 m of the water column and the drifters had minimal windage. A Garmin Etrex 10 GPS device was attached to each drifter using a small waterproof bag. The GPS units were set to record points at a set time interval (1 s at Mumbles Head, 2 s at Ramsey Sound due to memory on the GPS and fieldwork duration). Latitude and longitude were converted to UTM easting and northings, and then change in position calculated and converted to speed using the recorded timesteps. The accuracy of position or speed estimates was not assessed for these GPS units: the units typically have absolute positional accuracy of 3–6 m, however relative positional accuracy over the short-term is much higher [87]; previous studies using similar units have suggested that the majority of speed errors are within ± 0.2 m s^{-1} [88–90] and a mean error of 0.01 m s^{-1} has been reported [90]. Presence of drifters in the field of view equates to artificial seeding which might have been expected to skew results; however comparison between videos with and without drifters showed no difference [91].
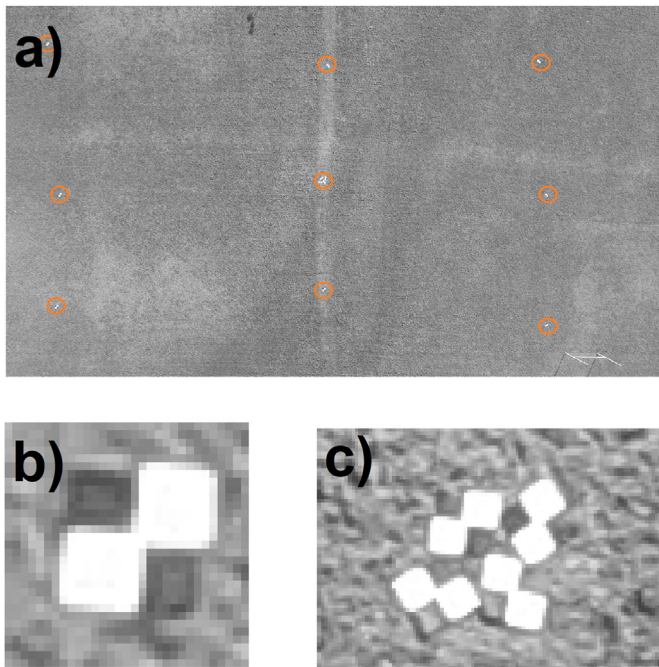
Fig. 4. a) the grid set out for the stability tests (targets ringed in orange); b) a close up of the black and white quadrant targets; c) a close up of the central target used for the cross-correlation.
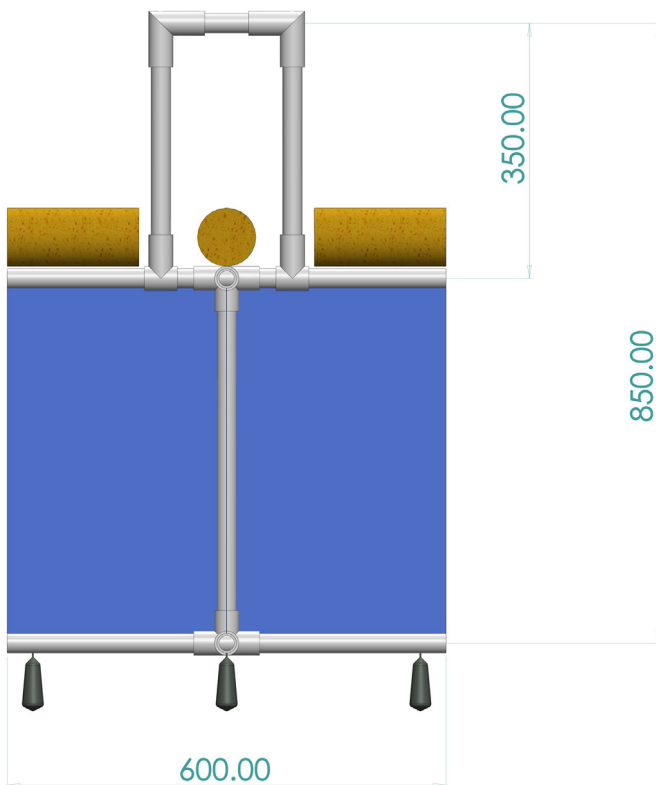

Fig. 5. The design of the low-cost Lagrangian surface drifters: the blue indicates the tarpaulin drogue (i.e., "sail" to capture flow beneath the sea surface); the grey the PVC piping frame; the yellow the 'pool noodles' used for buoyancy; and the black represents the fishing weights used to provide stability. Dimensions are in mm.

At Ramsey Sound, ADCP transects were conducted from a 10 m monohull vessel using a downward orientated Teledyne Sentinel operating at 600 kHz. Data were acquired using WinRiver II software, with GPS and wind data measured by an AIRMAR 200WX meteorological station. The ADCP was configured to collect 0.5 m bins to a depth of 50 m, pinging at 2 Hz, alternating between water profile and bottom track pings which enabled correction for pitch and roll. A compass calibration was carried out before data collection to remove the magnetic signature of the vessel. The ADCP was mounted on the side of the vessel at a depth of 0.5 m and with the first bin starting at 0.82 m below surface; therefore, the validation data considered were between 0.82 and 1.32 m below surface. ADCP transects were collected covering the flight areas immediately before and after drone flights. Error estimates from the ADCP gave a mean error in velocity of 0.19 m s^{-1}.

ADCP transects were obtained at the Pentland Firth immediately after the drone flights, using the MV Aurora, a small 7 m catamaran vessel, the same vessel that was used to launch the drone. A similar ADCP was used to Ramsey Sound (Teledyne Workhorse Sentinel 600 kHz), which was configured to ping at 2 Hz, also alternating between water profile and bottom track pings. Bin depths were 2 m. The considered bin in this analysis equated to 2.66–4.66 m below the surface due to instrument mounting depth and blanking distance. D-GPS position was collected with the underway ADCP data using a Hemisphere VS131 differential GPS system with Teledyne RDI VMDAS software. Bottom tracking was implemented correcting ADCP data for boat movement. Error estimates from the ADCP gave a mean error in velocity of 0.18 m s^{-1}.

All measured validation data were highly variable in time and therefore a temporal moving average filter, with a window length of 10 s, was applied to smooth data prior to comparison with the PIV data. Since the validation data collection was mobile transects or tracks, this is a smoothing in space as well as time.

3.3. PIVlab method analysis

Images were transformed to greyscale and contrast stretched with a saturation of 2% before contrast limited adaptive histogram equalisation [92] applied with a window size of 40 x 40 pixels; the window size was determined from preliminary analysis of Mumbles Head data. This pre-processing emphasised the features on the water surface.

PIVlab was used to conduct the analysis, with the default fast Fourier transform window deformation algorithm, standard correlation robustness and the Gaussian 2x3 point estimator for sub-pixel movement [60]. Velocities were transformed from pixels/s to ms^{-1} using the ground sampling distance. Returned velocities were filtered using a threshold of 8-times standard deviation and manual definition of velocity limits within the PIVlab GUI to remove clear outliers. Values were attributed to invalid data points via interpolation between valid velocities. The mean of all individual frame-on-frame velocities over a 60 s video segment was then taken to be the velocity for each video.

To establish the appropriate pixel size for the interrogation area, a range of values were tested and root mean square error (RMSE) calculated against drifter data for a section of video from Ramsey Sound with mean drifter velocity of 1.35 m s^{-1} (standard deviation 0.5 m s^{-1}). A three pass analysis was conducted, with windows reducing by half every pass. Smaller starting window size slightly increases accuracy of results (Table 2), therefore a starting pixel window of 128 px was used with subsequent passes of 64 px and 32 px. It should be noted that reducing size of the interrogation area does increase computational time.

The ground sampling distance for data from the Phantom was 0.0505 m whereas the ground sampling distance for data from the

Table 2
Root mean squared errors depending on the size of the starting window in pixels (px).

Run (px)	100	200	250	300	350	500
RMSE (ms^{-1})	0.209	0.218	0.221	0.222	0.224	0.229

M210 was approximately 0.03 m (depending on exact flight height and tide level). This meant that, at 30 fps, the velocity equivalent to a movement of 1 pixel between frames was 1.52 m s^{-1} (Phantom) and 0.9 m s^{-1} (M210); while there is sub-pixel estimation within PIVlab, to reduce this speed associated with movement of 1 pixel, frames were extracted at 15 fps such that 1-px movement between frames equated to 0.45 m s^{-1} (M210) and 0.76 m s^{-1} (Phantom).

Video lengths of 60 s were used in the analysis. This decision was based on a trade-off between an industry requirement for rapid area mapping (shorter videos) and the turbulent flows at tidal stream sites requiring sufficient temporal averaging to obtain reasonable estimates of mean current. The 60 s duration was determined based on consideration both of 2009 bottom-mounted ADCP deployment at Ramsey Sound (Fig. 6) and comparison of results of different video segment lengths (see section 4.3). Measurements from the ADCP bin closest to the surface were extracted for 15 min every hour and then the percentage error between averages over different temporal windows and the 15 min time average calculated. Unsurprisingly, longer time windows led to lower percentage errors (Fig. 5); for a 60 s time window, the average percentage error was 7%. It should be recognised that the use of drones to map surface currents is more akin to an ADCP transect (where minimal temporal averaging is accepted as standard) than a fixed ADCP deployment.

4. Results

4.1. Stability and georeferencing analysis

The stability of the M210 drone was assessed for a range of windspeeds (Fig. 7). Mean values of frame-on-frame movement were calculated and then converted to error in ms^{-1}. Mean frame on frame movements ranged from 0.003 m to 0.01 m; this is an average of less than one pixel ground sampling distance at 120 m altitude. Converting to error gave a mean value of 0.07 m s^{-1} with a maximum of 0.15 m s^{-1}. There is no significant relationship between windspeed and drone movement; it is likely that wind
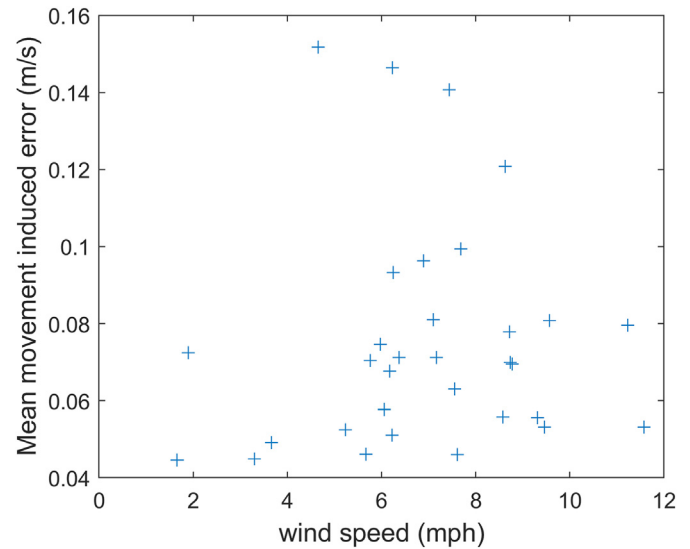

Fig. 7. A plot of error arising from drone stability against wind speed.

gustiness and turbulence are more relevant to the small movements observed.

Average geo-referencing error was 2.1 m (standard deviation 3.2 m) for non-RTK flights; it is assumed that this would reduce for RTK-enabled flights but has not been tested. Errors are smallest at the central point, with slightly larger errors near the edges of the image.

4.2. Drifter and ADCP validation measurements

Histograms of velocity measurements for all sites using both drifters and ADCP data are given in Fig. 8. A range of flow speeds have been measured, up to almost 2.5 m s^{-1}. Tidal turbine cut-in velocities and rated velocities vary depending on design; cut-in speeds in the literature range from 0.5 m s^{-1} − 1 m s^{-1} (average 0.88 m s^{-1}) and rated velocities between 2 and 4 m s^{-1} with a mean of 2.91 m s^{-1} [93]. Therefore, the validation data cover a sensible range for this application, although generally at the lower end of velocities of interest and some velocities below typical cut in speeds. The top bin of the ADCP datasets does not measure the true surface; typically, one would expect the true surface current to be
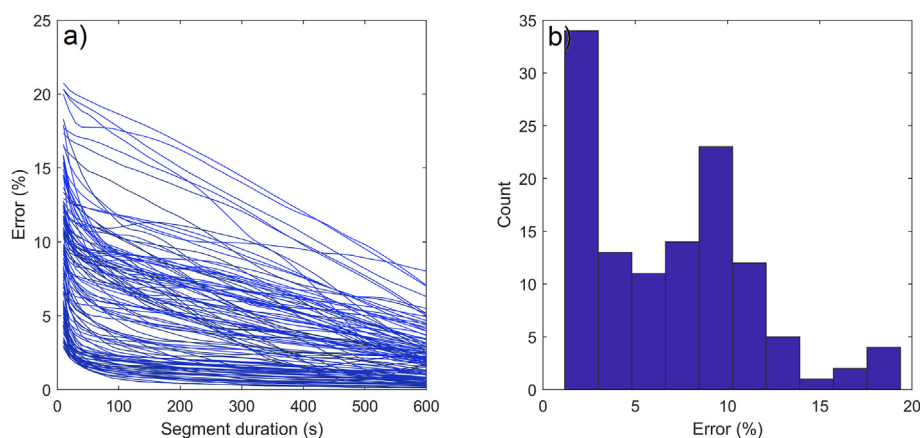

Fig. 6. a) Percentage error with reference to 15-min mean velocity against segment duration for the uppermost bin of a bottom mounted ADCP, lines are shaded based on mean velocity such that higher velocities are darker blue; b) a histogram of percentage errors for segments of 60 s duration using the same ADCP data.
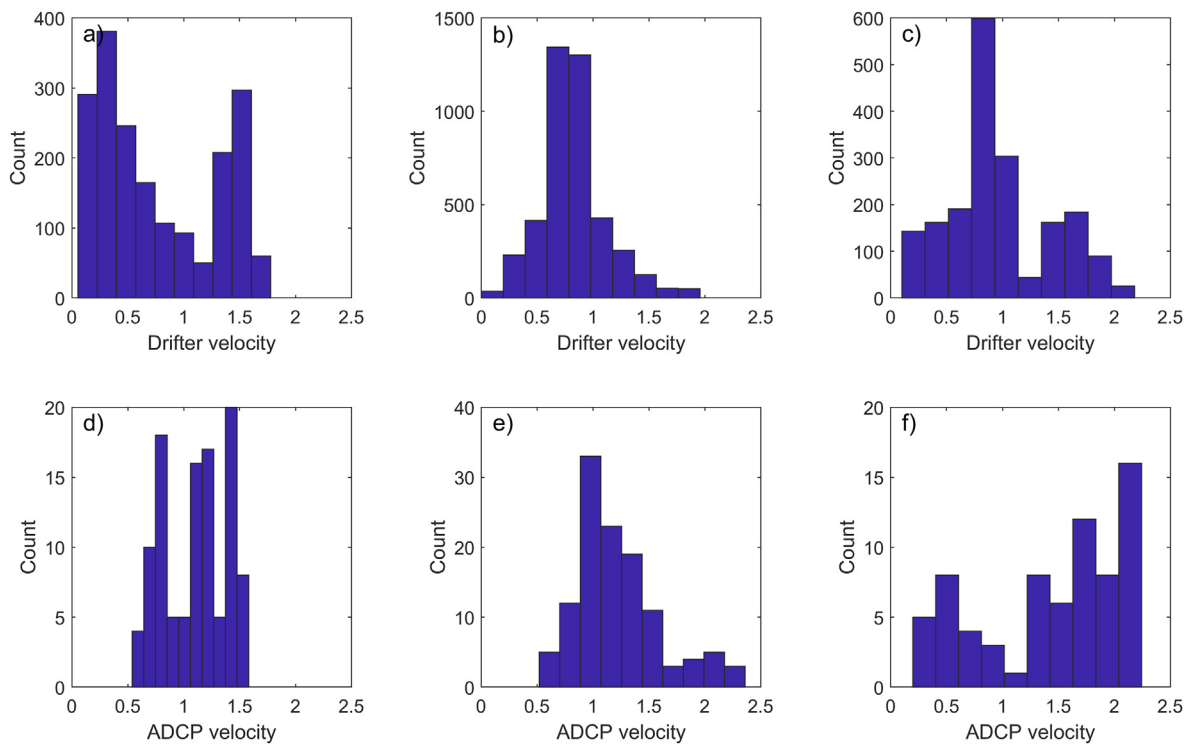
Fig. 8. Histograms of validation data speeds for: a) drifters at Mumbles Head; b) drifters at Ramsey Sound on 12/05/2021; c) drifters at Ramsey Sound on 14/05/2021; d) ADCP at Ramsey Sound on 12/05/2021; e) ADCP at Ramsey Sound on 14/05/2021; f) ADCP at the Inner Sound of Pentland Firth.
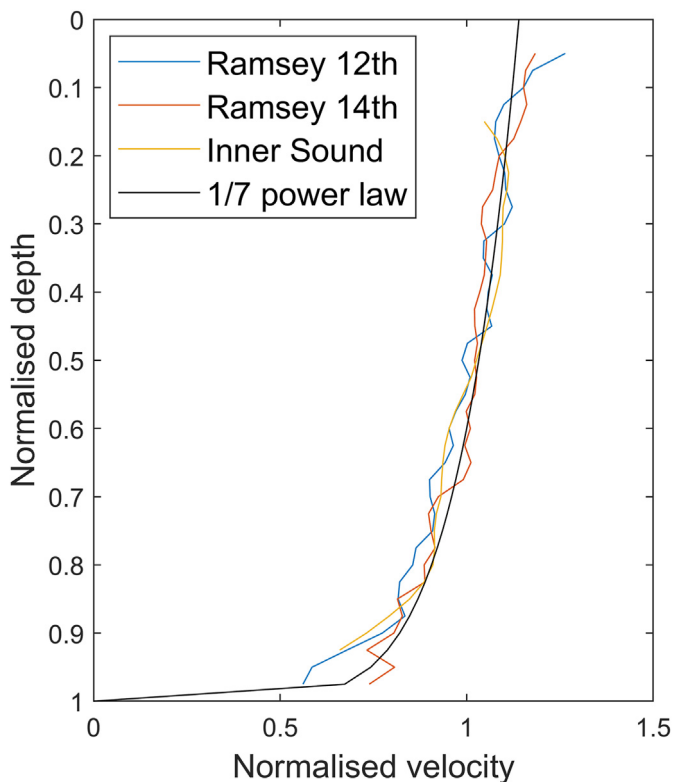

Fig. 9. Mean velocity profiles. To best represent the profile shape, velocities were normalised by mean velocity and depths by ADCP-measured water depth prior to the mean being taken. A 1/7th power law current estimation is also shown.

higher. To illustrate this, Fig. 9 shows the mean of profiles that have had velocities normalised by mean profile velocity and depths normalised by depth to seabed (measured by ADCP) to give a representation of average current profile. Additionally, a 1/7th power law profile is included using a bed roughness of 0.4, a value previously estimated as suitable for tidal stream site velocity profiles [94]. The motivation for using a previously estimated bed roughness value, rather than curve fitting to obtain a value, is the desire to be able to estimate water column velocities from surface velocities without prior water column velocity information (see Section 4.6). There is an interesting difference between data from Ramsey Sound on the 12th May which seems to show a larger increase in current speed near the surface, compared to the 14th May. This difference is postulated to be caused by the greater wind speeds on the 12th May. The top bin of data in the Inner Sound is lower in the water column and so it is harder to determine response nearer the surface, but higher velocities are expected based on the power law fit.

4.3. Example surface current maps

Fig. 10 provides two examples of surface current maps averaged over a 60 s video, one from Mumbles Head and one from Ramsey Sound. Drifter measurement locations and direction are shown as the grey arrows. The smaller scale of the site at Mumbles Head (Fig. 8a) means that the current jet between the islands and the adjacent lower flow region can be seen in one field of view. For Ramsey, while site scales are much larger, variation in current over the area is still observable. While not the focus of this work, which considers current magnitude, it is relevant to consider current direction. In both cases, current directions of surface velocimetry outputs and drifters match well; there is more variability in the drifter directions, but this is to be expected given they are instantaneous directions rather than 60 s averages for the current maps.
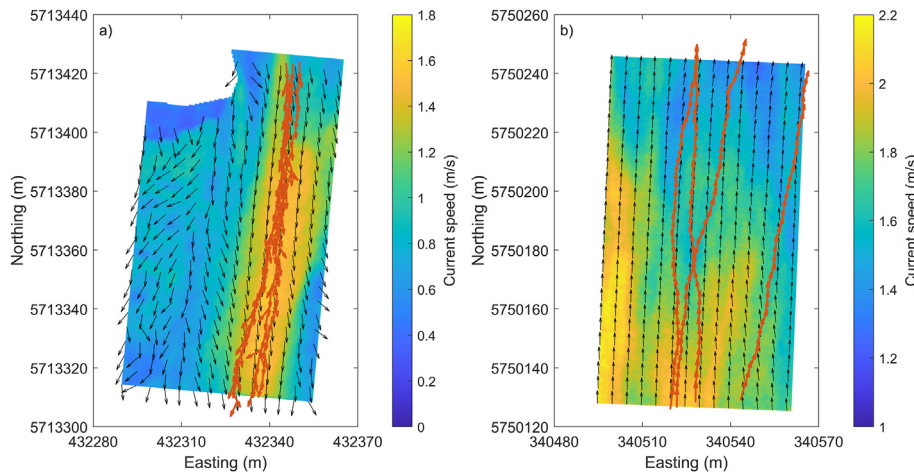
Fig. 10. Example LSPIV surface velocity maps for one 60 s video segment for: a) Mumbles Head and b) Ramsey Sound. Colour shading indicates current speed and black arrows are unit vectors representing LSPIV estimated direction. The orange arrows are unit vectors indicating direction of drifter travel. The masked out section in panel a) is a section of land in the field of view.

4.4. Comparison between PIV results and measured flow data

To determine whether 60 s was an appropriate video length for analysis, root mean square errors (RMSE) were calculated for different video lengths for a subset of the Ramsey Sound data (Fig. 11). It can be seen that mean RMSE drops as video length increases, but that the rate of decrease slows around 50—60 s; thereby suggesting that the chosen duration is appropriate and a suitable compromise between rapid surveying of large areas and more accurate mean flow values.

Comparison between ADCP measurements and PIVlab-derived currents for the two Ramsey Sound experiments and the Inner Sound experiment is given in Fig. 12. ADCP and PIVlab measurements show good correlation for the experiment at Ramsey Sound on the 14th May and reasonable correlation at the Inner Sound. The
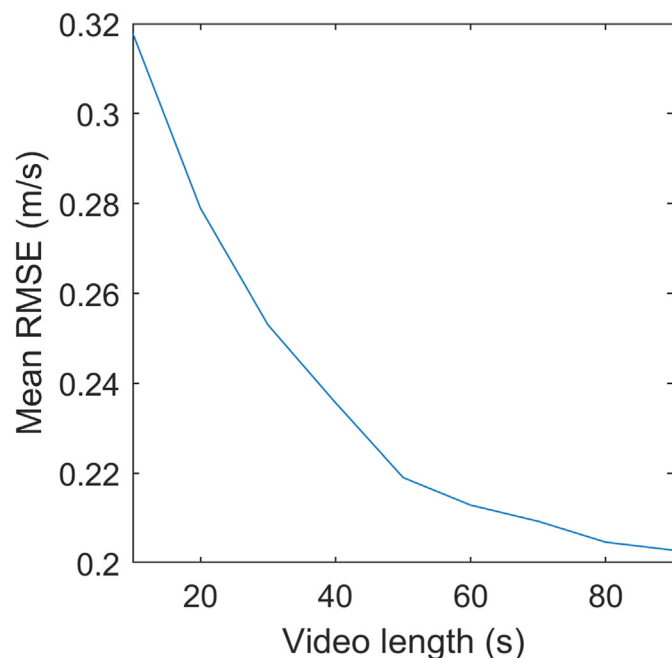
relationship is poorer at Ramsey Sound on the 12th May. The scatter is greater for the Inner Sound and there seems to be a bias with PIVlab overestimating compared to the ADCP, a similar bias is shown at Ramsey on the 12th May. These biases may be related to the ADCP not measuring true surface currents, which are likely to be higher (Fig. 9). The bias is smaller and in the other direction for the 14th May, possibly related to less noticeable wind effects (Fig. 9).

Correlation and error statistics are shown in Table 3. Values are given for all instances and for measured values above 0.88 m s^{-1} (the mean cut-in speed for tidal stream turbines) to represent the velocities most relevant to the tidal stream turbine industry. For all three experiments, consideration of velocities over 0.88 m s^{-1} reduces the RMSE, however r^2 values are only improved for the experiment at Ramsey Sound on the 14th May. Results at all sites are similar in terms of percentage errors when only higher velocities are considered but quite different when lower velocities are also included. Percentage errors and RMSE are both reduced when higher velocities only are considered. There is less difference for Ramsey Sound on the 14th May; results in general are best for this case. Correlation is highest for Ramsey on the 14th May and worst for Ramsey on the 12th May, despite error statistics on the 12th been better than for the Inner Sound. Importantly, the RMSEs calculated are much less than the variability in measured flow over the tidal cycle. Additionally, in the error calculations, it is assumed that the validation data represents the true velocity, when in fact there is an error associated with both ADPC and drifter measurements (see Discussion).

Fig. 13 gives the same comparison for the drifter velocities. Both the comparison against each drifter measurement and the drifter track mean measurements are displayed; the RMSE, r^2, and percentage error values are given in Tables 4 and 5. On average, comparison with surface drifters (Tables 4 and 5) give better performance than comparison with ADCP (Table 3). One can see different clusters on the 12th depending on whether measurements were taken on the flood or ebb. The data on the ebb shows PIVlab consistently underestimating compared to the validation data; the PIV estimate is almost giving a straight line result, suggesting it is insensitive to current velocity. However, higher velocities are not covered in the ebb tide data and so performance may improve if tests done for higher ebb tide velocities. On the flood tide, PIVlab and drifter velocities match well for higher velocities but PIVlab overestimates for lower velocities. A similar
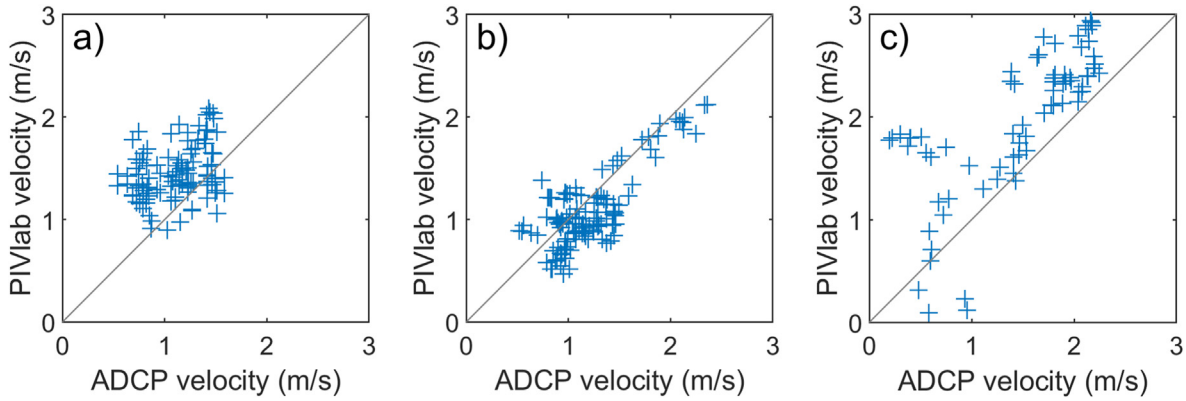

Fig. 11. Mean RMSE of PIVlab results compared to surface drifters against video length for a subset of the Ramsey Sound data covering velocities from 0.8 to 1.5 m s^{-1}.

Fig. 12. PIVlab derived velocity against ADCP measured velocity for: a) Ramsey Sound on 12/05/21, b) Ramsey Sound of 14/05/21, and c) the Inner Sound of the Pentland Firth.

Table 3
RMSE and r2 values for comparison between PIVlab results and ADCP for all flow conditions ("all") and flow speeds important for tidal-stream energy resource, when flow speeds are above the threshold of turbine generated electricity ("v > 0.88 m s^{-1}"). Values for the individual sites and an average value are presented.

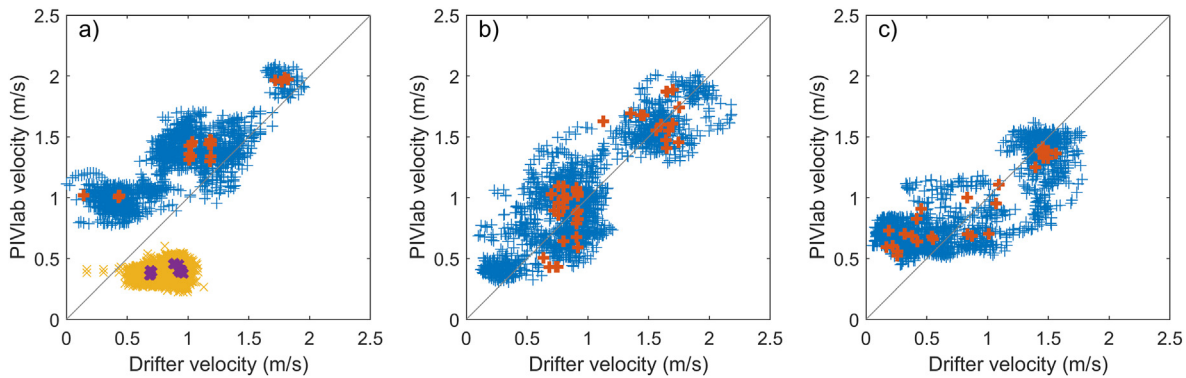| Site	Velocity set	RMSE (ms^{-1})	r^2	Mean percentage absolute error
Ramsey (12/05/21)	All	0.46	0.10	42%
Ramsey (12/05/21)	v > 0.88 m s^{-1}	0.35	0.07	24%
Ramsey (14/05/21)	All	0.28	0.60	22%
Ramsey (14/05/21)	v > 0.88 m s^{-1}	0.27	0.70	18%
Inner Sound	All	0.68	0.56	75%
Inner Sound	v > 0.88 m s^{-1}	0.54	0.65	28%
Average	*all*	*0.47*	*0.42*	*46%*
Average	*v > 0.88 m s^{-1}*	*0.39*	*0.47*	*23%*

Fig. 13. PIVlab derived velocity against surface drifter measured velocity for: a) Ramsey Sound on 12/05/21, b) Ramsey Sound of 14/05/21, and c) Mumbles Head. Instantaneous velocities are given as the finer blue crosses and track mean values as the thicker red crosses. For the experiment on the 12th (b), data are split between flood and ebb with yellow and purple indicating the ebb.

Table 4
RMSE and r^2 values for comparison between PIVlab results and instantaneous drifter velocities for all flow conditions ("all") and flow speeds important for tidal-stream energy resource, when flow speeds are above the threshold of turbine generated electricity ("v > 0.88 m s^{-1}"). Values for the individual sites and an average value are presented.

Site	Velocity set	RMSE (ms^{-1})	r^2	Mean percentage absolute error
Ramsey (12/05/21) -Flood	All	0.39	0.92	72%
Ramsey (12/05/21) − Flood	v > 0.88 m s^{-1}	0.29	0.92	25%
Ramsey (12/05/21) − Ebb	All	0.41	0.05	48%
Ramsey (12/05/21) − Ebb	v > 0.88 m s^{-1}	0.54	0.01	57%
Ramsey (14/05/21)	All	0.24	0.74	30%
Ramsey (14/05/21)	v > 0.88 m s^{-1}	0.20	0.75	13%
Mumbles Head	All	0.34	0.65	106%
Mumbles Head	v > 0.88 m s^{-1}	0.27	0.43	15%
Average	*All*	*0.34*	*0.58*	*64%*
Average	*v > 0.88 m s^{-1}*	*0.32*	*0.52*	*28%*

Table 5
RMSE and r² values for comparison between PIVlab results and drifter velocities averaged over a track for all flow conditions ("all") and flow speeds important for tidal-stream energy resource, when flow speeds are above the threshold of turbine generated electricity ("v > 0.88 m s⁻¹"). Values for the individual sites and an average value are presented.

Site	Velocity set	RMSE (ms⁻¹)	r²	Mean percentage absolute error
Ramsey (12/05/21) -Flood	All	0.44	0.67	70%
Ramsey (12/05/21) − Flood	v > 0.88 m s⁻¹	0.33	0.29	23%
Ramsey (12/05/21) − Ebb	All	0.45	0.17	51%
Ramsey (12/05/21) − Ebb	v > 0.88 m s⁻¹	0.52	0.55	56%
Ramsey (14/05/21)	All	0.22	0.76	19%
Ramsey (14/05/21)	v > 0.88 m s⁻¹	0.21	0.75	13%
Mumbles Head	All	0.25	0.85	57%
Mumbles Head	v > 0.88 m s⁻¹	0.14	0.85	9%
Average	*All*	*0.34*	*0.61*	*49%*
Average	*v > 0.88 m s⁻¹*	*0.30*	*0.61*	*25%*

pattern to the flood tide is seen at Mumbles Head. By contrast, on the 14th May at Ramsey Sound there is a good match for all measured velocities. The statistics are similar whether instantaneous or track mean velocities are considered. The similarity is lower when the Mumbles Head dataset is considered, possibly related to the presence of waves. RMSE values are worse for Ramsey Sound on the 12th May compared to the 14th May; this is also the case for the ADCP measurements and may be related to the stronger wind speeds on the 12th obscuring the current signal.

4.5. Consideration of errors

Given the scatter in the results, it is instructive to consider the relationship between errors and various factors. The factors considered were: error distribution about field of view; error against time difference between video recording and ADCP point; relationship between error and velocity; and, geographic distribution of errors. Fig. 14 shows percentage errors for both drifters and ADCP from all Ramsey Sound flights over both days, plotted in image co-ordinates. There is no obvious relationship between error and position in the image, indicating that any systematic errors caused by treatment of lens distortion or georeferencing are not a large source of discrepancy between LSPIV-derived and measured velocities.

One would expect errors to increase with temporal separation between video capture and ADCP measurement. Numerical model outputs from a validated model of the site [37] show current speeds varied by up to 0.35 m s⁻¹ over a 15-min period during the experiments, which is a similar magnitude to the calculated errors. Errors do increase with time (Fig. 15); however, the relationship is weak ($R^2 = 0.06$) and low errors are found even at longer temporal separation. This weak relationship suggests that validating the PIV results using ADCP transect data recorded within ±15 min of video

Fig. 15. A comparison between error and temporal separation of ADCP recording to video start time from the Ramsey Sound survey location. Dates correspond to the two survey dates in May 2021.

capture is not a major source of the scatter seen in the results. The ADCP data on the 12th May had greater temporal separation from the videos than that on the 14th May which may go some way to explain the worse correlation on the 12th May. The same graph was not produced for drifters since the drifters were largely time synchronous with the video.

There appears to be a structure to the errors when comparing against measured velocity (Fig. 16); in this case error is displayed in ms⁻¹ rather than percentage error. For all experiments and validation data types, there is a negative trend, though the slope varies. The trend is statistically significant at the 99% level for all cases except for the Inner Sound ADCP (significant at 90% level) and the Ramsey Sound 14th May drifter data (insignificant). For these two, the trend is not visually obvious. Errors are positive (PIVlab over predicting) for lower velocities and either lower magnitude or negative (PIVlab underpredicting) for higher velocities. The exception is the ebb tide results for the 12th May at Ramsey Sound where errors are always negative, but there is still a significant negative trend.

Percentage error for ADCP and drifter results were mapped for both days at Ramsey Sound (Fig. 17), only the flood was considered
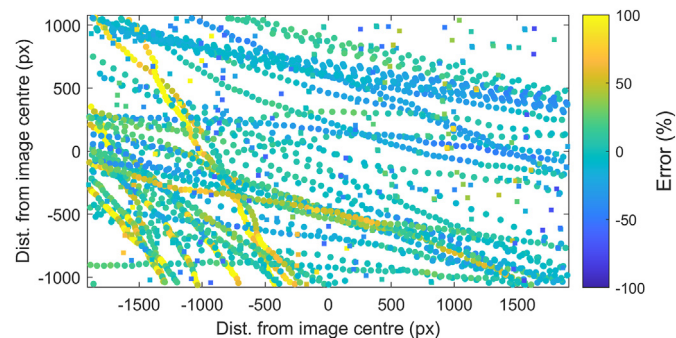
Fig. 14. Percentage errors for all ADCP and drifter tracks from Ramsey Sound plotted on image co-ordinates. Circles indicate drifter points and squares ADCP points.
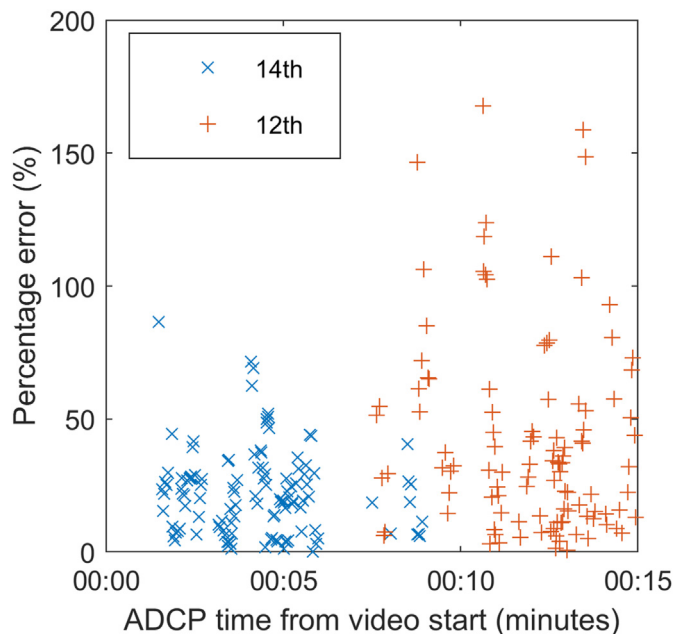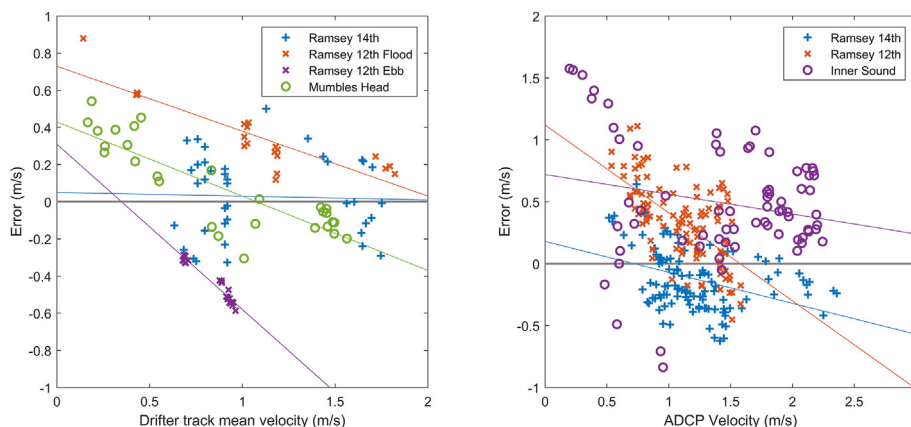
Fig. 16. Plots of error against validation velocity for: a) surface drifters as track mean values; b) ADCP. Lines of best fit are added to the figure, in the same colour as the icons.
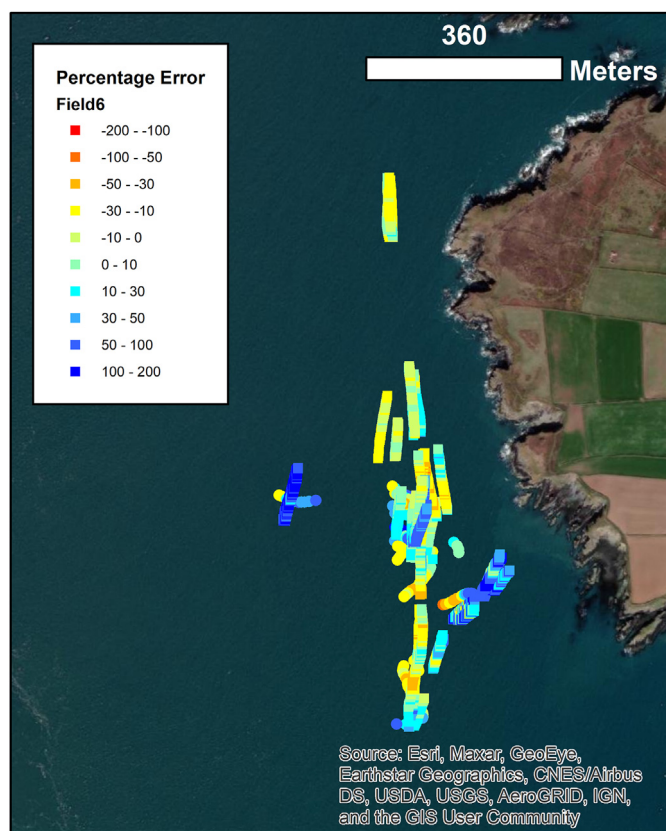

Fig. 17. A map showing the geographic distribution of errors for both days at Ramsey Sound (flood only).

Fig. 18. Pixel timestacks for greyscale intensity, timestacks are orientated such that the current direction is from left to right. a) Mumbles Head; b) Flood from Ramsey Sound 12th; c) Ebb from Ramsey Sound on the 12th; d) Flood from Ramsey Sound on the 14th. Where the current is evident, orange lines illustrate the travel of some current signatures; in panel a, the blue lines indicate wave signatures in the timestack.

as there was minimal spatial variation for the ebb results. There is nothing too striking in the geographic spread of errors; there is greater positive percentage error to the east, out of the main flow which matches the findings shown in Fig. 16. The positive errors in the centre of the sound are from runs close to slack water.

Given that errors are greater at low flow, something that has been noted in fluvial environments too, it is worth considering the source of these errors. One aspect is the presence of contaminating signals from wind-driven ripples or waves that are of greater magnitude than the current signature. Fig. 18 shows pixel intensity timestacks for sections of video from Mumbles Head, from both flood and ebb at Ramsey on the 12th May and from Ramsey Sound
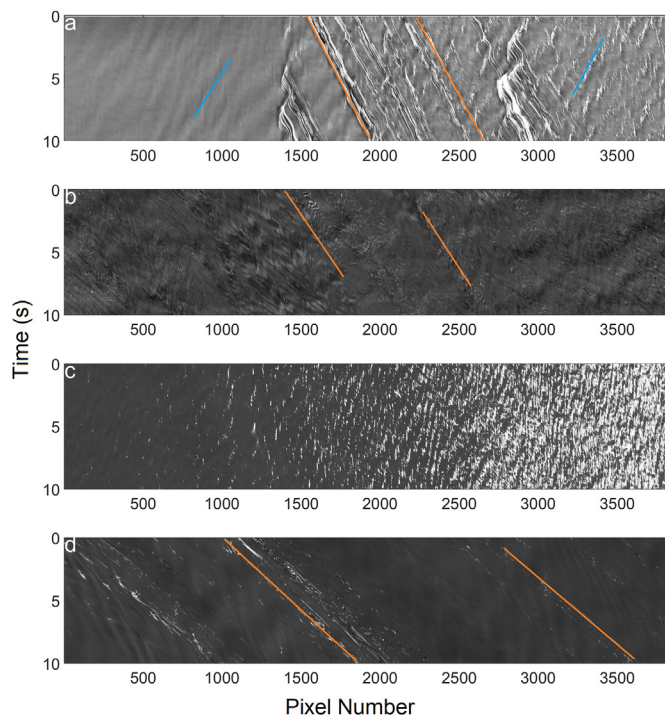
on the 14th May. Pixel intensity timestacks are created by 'stacking' 1 − pixel wide transects taken from consecutive frames in the same location; thus, they show the time evolution of greyscale intensity and the movement of features through times can be tracked. For these timestacks, the transect runs parallel to the current. At Mumbles Head the wave signature (right to left) can be seen and is similar in both greyscale intensity variation and velocity (gradient in figure) to the current signature (left to right) for much of the image slice and greater in intensity than the current signature for pixels 1−1400. Likewise, for the flood tide at Ramsey Sound on the 12th May, while the left to right current signal is more evident, there is still a right to left signal caused by small waves which is not dissimilar in magnitude. On the ebb tide, sun glint off wind ripples means that a current signal is not evident at all. By contrast, the

example from the flood tide on the 14th May shows a more dominant current signal compared to the wave signal. For better understanding of the variation in flow signatures, embedded videos are provided in Appendix A.

4.6. Translation to currents at depth

The ability to translate from drone-measured surface currents to currents deeper in the water column without existing information of the velocity profile would be highly desirable. This is tested here based on the similarity between mean normalised ADCP profiles and a 1/7th power law profile with coefficients estimated at other sites [94] (Fig. 9). The power law profile was used with the surface current estimate to estimate currents 10m above the sea bed by setting z to 10 in the power law profile equation:

$$U_z = \left(\frac{z}{\beta \, h}\right)^{1/7} \overline{U}$$

Where U_z is the current speed at a height z above the seabed; β is the bed roughness, set to 0.4 based on [94]; h is the total water depth (in this case as measured by ADCP); and, $\overline{U}$ is the mean current speed estimated as 1.1139 x $U_{surface}$ (based on the normalised current profile in Fig. 9). This calculated velocity was compared to the velocity at 10m above the sea bed measured by the ADCP. Fig. 19 displays the results of this analysis. For both the Ramsey Sound cases, accuracies are similar: on the 12th May RMSEs are actually lower than the surface current comparison (RMSE = 0.32 m s^{-1} versus 0.46 m s^{-1}), which suggests a spurious result for this date; on the 14th May, where good comparison at the surface was found (RMSE = 0.28 m s^{-1}), the RMSE is only slightly worse (0.32 m s^{-1}). Results are less good for the Inner Sound, where currents are overestimated. This is related to the overestimation of surface currents.

5. Discussion

This work has demonstrated the use of large-scale particle image velocimetry applied to drone collected video for measurement of surface currents at tidal stream sites and investigated the magnitude and source of errors. It is important to note that the validation data (ADCP and drifters) were assumed to represent the true surface velocity but in fact have errors associated with them; both data types have errors of approximately 0.2 m s^{-1}. Overall, the method was least successful at Ramsey Sound on the 12th May when data were collected at the limit of drone wind endurance (wind 31 km/h during experiment, maximum endurance 35 km/h); which meant there was strong wind generated signals in the imagery. Excessive wind or wave generated surface phenomena can become the dominant signal; cross-correlation tracks these rather than the current features and hence provides erroneous results. Results are best for the experiment at Ramsey Sound on the 14th May. For this experiment, the wind was much lighter (10 km/h) and thus contaminating wind generated signals were lower; additionally, cloudless skies meant illumination was both bright and uniform which meant turbulent surface structures were highly visible. However, differences in accuracy are noted between the flood and ebb tide results on the 12th May when there is no difference in wind speeds, but wind-driven ripples are more obviously dominant for the ebb. Therefore, it is postulated that accuracy will also depend on upstream bathymetry and its effect on turbulent structures on the surface. At the Inner Sound there is a large amount of scatter; it is postulated that the very smooth areas in kolk boils lead to areas where there are no trackable features, leading to poor PIV performance when boils are present in the

images. Additionally, the larger scale of the Inner Sound's mean weather effects on signal to noise ratio are likely to be greater.

Accuracy increases when only velocities above a typical tidal stream turbine cut-in speed (0.88 m s^{-1}) are considered. This is encouraging because it means that for the velocities most of interest, large scale particle image velocimetry is more likely to give reasonable results. However, since lower velocities are typically over predicted, areas of unsuitable current might be incorrectly assumed to be worth further exploration. From a site viability assessment perspective this means that one might expect some false positives but few false negatives. However, it should be noted that turbine power output is proportional to the cube of velocity so any errors in velocity will be magnified when power is estimated.

A range of error statistics have been reported for surface velocimetry in fluvial environments. Using PIVlab, Liu et al. [66] report a mean absolute error of 0.97 m s^{-1} for flows around 2 m s^{-1} and a drone elevation of 112 m; they found that mean absolute error reduced to 0.49 m s^{-1} when the drone was flown at 32 m altitude (finer pixel resolution). By contrast, in flows below 1 m s^{-1}, Lewis et al. [68] found that velocity magnitudes measured by PIVlab were within 5% of near surface velocities measured by acoustic Doppler velocimeter (ADV). Another LSPIV study compared drone and fixed video results and found errors of around 50% [95]. Lower errors are found with seeded experiments, for example, Strelnikova et al. [96] report RMSE values of 0.1 and mean absolute percentage differences of 12%. The results presented here for tidal stream sites are similar to the range of results presented for fluvial applications. This is encouraging given that there are a range of factors that, with further research, could be improved upon.

It is suggested that image manipulation to identify and remove contaminating signals would improve results. Future research will consider appropriate filtering mechanisms to achieve this. There are a range of other surface velocimetry techniques which may provide better results and future work will also examine the applicability of these. It has been shown that accuracy is dependent on the site characteristics and so work is underway to collect data at a wide range of sites.

Greater computational power may also enable better results; due to use of desktop PCs, the 'standard' correlation robustness setting in PIVlab was used [61]. 'High' and 'extreme' correlation robustness settings in the software provide alternative, more accurate (lower RMSE), approaches to the cross-correlation but at expense of increased computational time; approximately 2–3 times slower for the 'high' setting and 7 times slower for the 'extreme' setting [61].

One aspect of the approach that will, in general, be less accurate than for fluvial applications is the georeferencing, due to the lack of ground control at tidal sites (typically river banks are in the field of view for fluvial studies). However, stability assessment has shown that frame on frame movement leads to average errors in current velocity of 0.07 m s^{-1}; for the velocities of typical interest to tidal stream developers (0.88–4 m s^{-1}) this equates to percentage errors of 2–8%. This hovering stability induced error is similar to previously reported for a different drone, the DJI Phantom 3 [68]. Moreover, as the drone aims to keep station in one location, some movements will lead to over-estimation and others under-estimation of currents which will mean errors in returned velocity will be less when averaged over 1 min. It is feasible that with real time kinematic (RTK) GPS, the drone's position could be used to correct for any hovering instability; RTK precision can be as fine as 0.01 m and at 120 m elevation the ground sampling distance is 0.03 m. Limitations in the flight log data of the tested equipment meant this was not possible in this study but it could be possible with other systems. Average absolute x,y, positioning error compared to GPS was found to be 2.1 m based on targets spread out
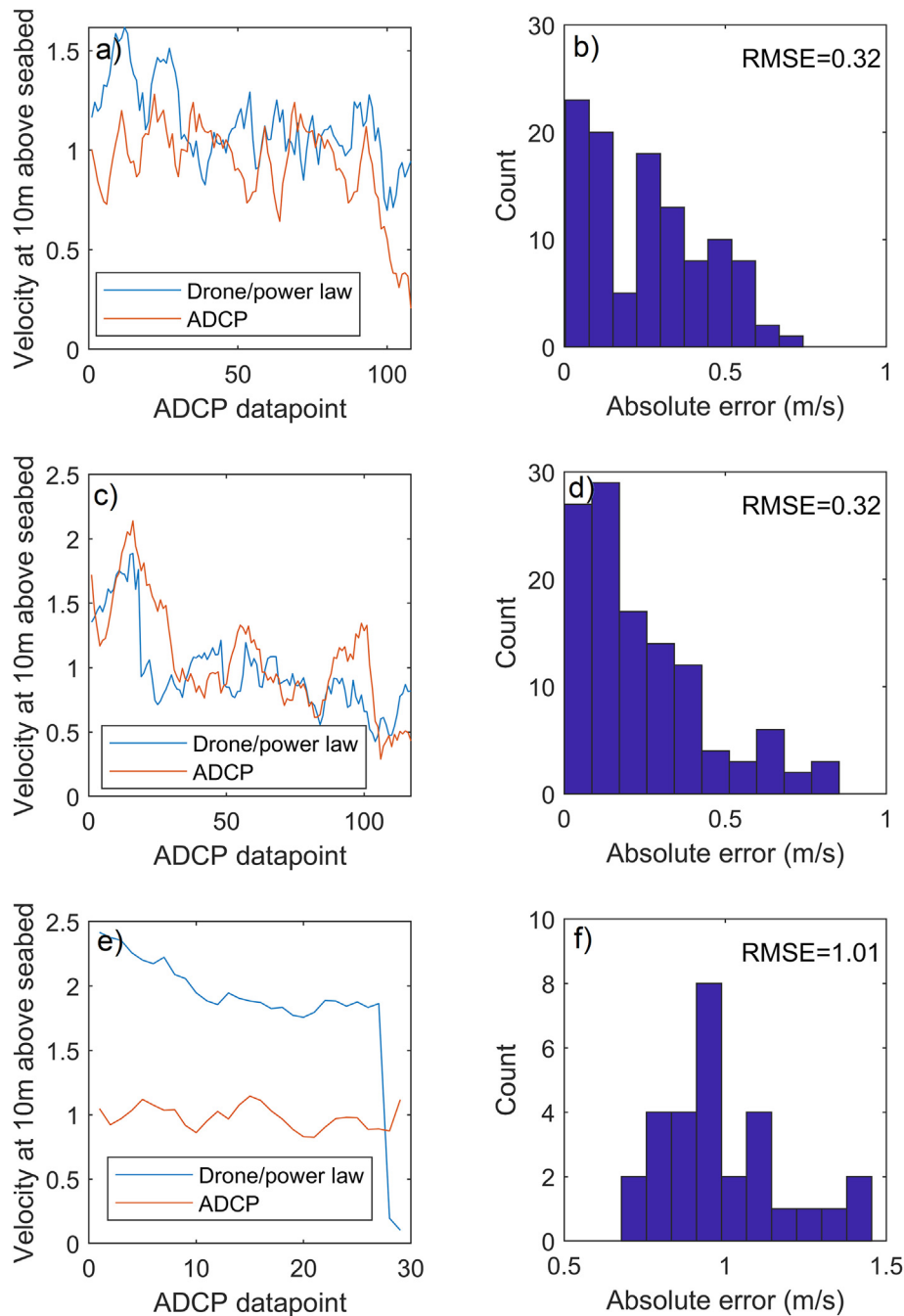
Fig. 19. A comparison between ADCP velocities measured at 10m above the seabed and velocities at 10m above seabed estimated from drone measured surface velocities and the power law profile. Comparative plots of the two velocities are given for a) Ramsey Sound on the 12th May, c) Ramsey Sound on the 14th May, e) Inner Sound. Error histograms are given for b) Ramsey Sound on the 12th May, d) Ramsey Sound on the 14th May, f) Inner Sound.

through the image. It is considered that this absolute accuracy is acceptable, given the scales at tidal stream energy sites. The errors were lower for the central targets than targets nearer the edges of the image, suggesting that lens distortion may not be completely removed. Additionally, georeferencing was sensitive to the accuracy of the elevation estimate which affected ground sampling distance; this would also give larger errors further from the centre of the image. The accuracy of the ground sampling distance estimate will also affect the accuracy of the returned velocity.

The work raises the question of the best way to validate the surface current maps derived from PIV. Results are slightly better

for the surface drifters, which is unsurprising since they better map the true surface currents due to ADCP blanking distance. However, the movement of surface drifters mean averaging over the same 60 s duration as the PIV results is not really feasible while maintaining some spatial resolution; the same is true of ADCP transects. Bottom mounted ADCP allows appropriate temporal averaging, but, unless multiple devices are deployed, no spatial coverage. It might be that comparison of multiple remotely sensed techniques is more appropriate.

Knowledge of surface currents is important to the tidal stream industry, especially for floating tidal stream turbines. However, to

maximise benefit for developers of seabed mounted turbines, approaches to transform from surface currents to currents at hub height will be required. This needs further assessment, however, preliminary analysis (Figs. 9 and 19) suggests that a power law profile [94] can be used to transform surface velocities to the depth of interest, with accuracy largely depending on the accuracy of the initial surface current estimation. This approach does rely on also having suitable bathymetric information to assign the profile depth. Consideration will need to be given to deviation of current profiles from standard profiles at the near surface caused by wind-driven currents and Stokes drift; if suitable measurements are available these could be estimated and removed, alternatively it may restrict use of the technique to times with low wind and waves. This obviously has the advantage of improving accuracy of the results as well due to the aforementioned reasons.

Going forward, the ambition is to use the drone to collect videos with overlapping fields of view (such as presented in Fig. 8) creating a series of tiles that would cover an area of interest and when stitched together provide a wider area map. Such flights can be automated to ensure the correct area is covered, for example DJI drones can be controlled in 'mission' mode within the DJI Pilot app by providing a.kml file of desired hover locations and specifying the other flight and video parameters. Currently, in the UK, standard drone use is limited to visual line of sight (500 m) from the operator which limits the potential area mapped; however beyond visual line of sight permission is possible and in other countries, such as the EU, the 500 m limit is not currently required provided the drone can be identified visually. Another limitation is battery life; flight duration of the tested drones was 20—30 min, and it is for this reason that video segments were restricted to 1 min. Based on a 30 min flight, it is expected that 15 separate fields of view could be collected which, when flown at 120m above sea surface with a 10% overlap and a 3 x 5 grid would cover an area of 186 × 538 m. However, as drone and battery technology advances, newer drones have flight durations approaching 1 h, which means that either larger areas could be covered or longer video segments recorded which may better represent the mean flow (it was found that 1 min videos had errors of 7% compared to the 15 min mean flow). Therefore, in future it is imagined that wide areas could be mapped rapidly.

Additionally, while this work has focussed on average flow fields, it is possible that drones could also be used to consider other physics of surface flows such as turbulence. Here, frame on frame results were averaged, but individual frame on frame velocities could be considered to assess turbulent fluctuations. For such studies, longer videos would be needed to separate mean flow for turbulence; and, for accurate turbulence results, the station-keeping precision of drones would need to be improved or for movements to be mitigated for. This would be useful in better understanding the dynamics of features such as Kolk boils, which have been previously identified in drone imagery and linked to ecological behaviour [56,97]. Other studies have used optical imagery from drones to measure the surface wave field [98], based on the pixel intensity signal. It is also feasible that wave induced orbital velocities on the water's surface could be measured and this used to derive wave parameters. However, such measurements would likely need high seeding densities, whether natural foam tracers or artificial particles.

6. Conclusions

Nadir video data from low-cost, publicly available drones can be used to estimate sea-surface flow speed using surface velocimetry. Therefore, low-cost and low-risk remotely sensed tidal stream resource assessments can be made, greatly improving mapping of potential sites, particularly in challenging sites and remote communities/industries. The tested approach is complementary to existing ADCP techniques in terms of coverage, resolution, and accuracy.

Method accuracy was found to depend on site bathymetry generating sufficient surface turbulent structures that can be tracked, with differences noted between flood and ebb results at Ramsey Sound. Greater scatter in results was found for the larger Inner Sound compared to Ramsey Sound, which suggests site geometry may affect results, probably due to differences in site exposure and size of turbulent features. Accuracy was influenced by the presence of wind induced surface features. Under calm conditions at Ramsey Sound (10 kmh wind speed), the accuracy of velocities returned by large scale particle imagery are considered suitable for use in tidal resource estimation (RMSE <0.25 m s^{-1} versus surface drifters). Under windier conditions (31 kmh wind speed), current-advected surface features are partially obscured by temporally variable wind-driven surface features, leading to spurious cross-correlations and higher RMSEs (RMSE <0.54 m s^{-1} versus surface drifters). However, even under windier conditions, results can be suitably accurate for higher velocities (RMSE = 0.33 m s^{-1} against surface drifters), provided the turbulent surface structures are visible.

Data availability

The data underlying this article will be shared on reasonable request to the corresponding author.

CRediT authorship contribution statement

Iain Fairley: Conceptualization, Methodology, Validation, Formal analysis, Investigation, Writing — original draft, Writing — review & editing, Visualization, Funding acquisition. **Benjamin J. Williamson:** Conceptualization, Methodology, Investigation, Writing — review & editing, Supervision, Project administration, Funding acquisition. **Jason McIlvenny:** Methodology, Validation, Formal analysis, Investigation, Writing — original draft, Writing — review & editing, Funding acquisition. **Nicholas King:** Investigation. **Ian Masters:** Conceptualization, Writing — review & editing, Supervision, Project administration, Funding acquisition. **Matthew Lewis:** Methodology, Writing — review & editing, Funding acquisition. **Simon Neill:** Writing — review & editing, Funding acquisition. **David Glasby:** Methodology, Investigation, Visualization. **Daniel Coles:** Software, Resources. **Ben Powell:** Methodology, Investigation, Writing — original draft. **Keith Naylor:** Methodology, Investigation. **Max Robinson:** Methodology, Investigation. **Dominic E. Reeve:** Writing — review & editing, Supervision, Project administration, Funding acquisition.

Declaration of competing interest

The authors declare that they have no known competing financial interests or personal relationships that could have appeared to influence the work reported in this paper.

Appendix A. Supplementary data

Supplementary data to this article can be found online at https://doi.org/10.1016/j.renene.2022.07.030.

References

[1] IPCC, in: V. Masson-Delmotte, et al. (Eds.), Climate Change 2021: the Physical Science Basis. Contribution of Working Group I to the Sixth Assessment Report of the Intergovernmental Panel on Climate Change, 2021.
[2] A.S. Bahaj, Generating electricity from the oceans, Renew. Sustain. Energy Rev. 15 (7) (2011) 3399—3416.
[3] M.J. Khan, G. Bhuyan, M.T. Iqbal, J.E. Quaicoe, Hydrokinetic energy conversion systems and assessment of horizontal and vertical axis turbines for river and tidal applications: a technology status review, Appl. Energy 86 (10) (2009) 1823—1835.
[4] D. Coles, A. Angeloudis, D. Greaves, G. Hastie, M. Lewis, L. Mackie, J. McNaughton, J. Miles, S. Neill, M. Piggott, D. Risch, B. Scott, C. Sparling, T. Stallard, P. Thies, S. Walker, D. White, R. Willden, B. Williamson, A review of the UK and British Channel Islands practical tidal stream energy resource, Proc. Math. Phys. Eng. Sci. 477 (2255) (2021), 20210469.
[5] A. Pérez-Ortiz, A.G.L. Borthwick, J. McNaughton, H.C.M. Smith, Q. Xiao, Resource characterization of sites in the vicinity of an island near a landmass, Renew. Energy 103 (2017) 265—276.
[6] G. Todeschini, D. Coles, M. Lewis, I. Popov, A. Angeloudis, I. Fairley, F. Johnson, A.J. Williams, P. Robins, I. Masters, Medium-term variability of the UK's combined tidal energy resource for a net-zero carbon grid, Energy (2022) 238.
[7] S. Bhattacharya, S. Pennock, B. Robertson, S. Hanif, M.J.E. Alam, D. Bhatnagar, D. Preziuso, R. O'Neil, Timing value of marine renewable energy resources for potential grid applications, Appl. Energy (2021) 299.
[8] M. Lewis, J. McNaughton, C. Marquez-Dominguez, G. Todeschini, M. Togneri, I. Masters, M. Allmark, T. Stallard, S. Neill, A. Goward-Brown, P. Robins, Power variability of tidal-stream energy and implications for electricity supply, Energy 183 (2019) 1061—1074.
[9] A.S. Iyer, S.J. Couch, G.P. Harrison, A.R. Wallace, Variability and phasing of tidal current energy around the United Kingdom, Renew. Energy 51 (2013) 343—357.
[10] S.P. Neill, M.R. Hashemi, M.J. Lewis, Optimal phasing of the European tidal stream resource using the greedy algorithm with penalty function, Energy 73 (2014) 997—1006.
[11] N. Pearre, L. Swan, Combining wind, solar, and in-stream tidal electricity generation with energy storage using a load-perturbation control strategy, Energy (2020) 203.
[12] P.G. Novo, Y. Kyozuka, Tidal stream energy as a potential continuous power producer: a case study for West Japan, Energy Convers. Manag. (2021) 245.
[13] N. Carpman, K. Thomas, Tidal resource characterization in the Folda Fjord, Norway, Int. J. Marine. Energy 13 (2016) 27—44.
[14] M. Buric, S. Grguric, H. Mikulcic, X.B. Wang, A numerical investigation of tidal current energy resource potential in a sea strait, Energy (2021) 234.
[15] R. Cossu, I. Penesis, J.R. Nader, P. Marsh, L. Perez, C. Couzi, A. Grinham, P. Osman, Tidal energy site characterisation in a large tidal channel in Banks Strait, Tasmania, Australia, Renew. Energy 177 (2021) 859—870.
[16] N. Guillou, J.F. Charpentier, M. Benbouzid, The tidal stream energy resource of the Fromveur strait-A review, J. Mar. Sci. Eng. 8 (12) (2020).
[17] C.B. Jiang, Y.T. Kang, K. Qu, S. Kraatz, B. Deng, E.J. Zhao, Z.Y. Wu, J. Chen, High-resolution numerical survey of potential sites for tidal energy extraction along coastline of China under sea-level-rise condition, Ocean Eng. (2021) 236.
[18] A. Sentchev, T.D. Nguyen, L. Furgerot, P.B. du Bois, Underway velocity measurements in the Alderney Race: towards a three-dimensional representation of tidal motions, Phil. Trans. Math. Phys. Eng. Sci. (2178) (2020) 378.
[19] T.P. Wang, Z.Q. Yang, A tidal hydrodynamic model for cook inlet, Alaska, to support tidal energy resource characterization, J. Mar. Sci. Eng. 8 (4) (2020).
[20] A. Mohammadian, B. Morse, J.L. Robert, Assessment of tidal stream energy resources in a hypertidal estuary with highly irregular bathymetry using 3D numerical modelling, J. Ocean Eng. Marine. Energy. 5 (3) (2019) 267—281.
[21] M. Thiebaut, A. Sentchev, P.B. du Bois, Merging velocity measurements and modeling to improve understanding of tidal stream resource in Alderney Race, Energy 178 (2019) 460—470.
[22] S.L. Ward, P.E. Robins, M.J. Lewis, G. Iglesias, M.R. Hashemi, S.P. Neill, Tidal stream resource characterisation in progressive versus standing wave systems, Appl. Energy 220 (2018) 274—285.
[23] E. González-Gorbeña, A. Pacheco, T.A. Plomaritis, Ó. Ferreira, C. Sequeira, Estimating the optimum size of a tidal array at a multi-inlet system

[24] considering environmental and performance constraints, Appl. Energy 232 (2018) 292—311.
[24] D.S. Coles, L.S. Blunden, A.S. Bahaj, The energy yield potential of a large tidal stream turbine array in the Alderney Race, Phil. Trans. Math. Phys. Eng. Sci. (2178) (2020) 378.
[25] C.H. Frost, P.S. Evans, M.J. Harrold, A. Mason-Jones, T. O'Doherty, D.M. O'Doherty, The impact of axial flow misalignment on a tidal turbine, Renew. Energy 113 (2017) 1333—1344.
[26] M. Togneri, I. Masters, Micrositing variability and mean flow scaling for marine turbulence in Ramsey Sound, J. Ocean Eng. Marine. Energy. 2 (1) (2016) 35—46.
[27] Z.L. Hutchison, L. Lieber, R.G. Miller, B.J. Williamson, Environmental impacts of tidal and wave energy converters, in: Reference Module in Earth Systems and Environmental Sciences, Elsevier, 2021.
[28] J.J. Waggitt, P.W. Cazenave, R. Torres, B.J. Williamson, B.E. Scott, Quantifying pursuit-diving seabirds' associations with fine-scale physical features in tidal stream environments, J. Appl. Ecol. 53 (6) (2016) 1653—1666.
[29] I. Fairley, P. Evans, C. Wooldridge, M. Willis, I. Masters, Evaluation of tidal stream resource in a potential array area via direct measurements, Renew. Energy 57 (2013) 70—78.
[30] L. Goddijn-Murphy, D.K. Woolf, M.C. Easton, Current patterns in the inner sound (Pentland Firth) from underway ADCP data, J. Atmos. Ocean. Technol. 30 (1) (2013) 96—111.
[31] S.A. Brown, E.J. Ransley, S. Zheng, N. Xie, B. Howey, D.M. Greaves, Development of a fully nonlinear, coupled numerical model for assessment of floating tidal stream concepts, Ocean Eng. 218 (2020), 108253.
[32] I.E. Commission, Part 201: tidal energy resource assessment and characterization, in: TC 114 - Marine Energy - Wave, Tidal and Other Water Current Converters, 2015, p. 46.
[33] D.S. Mueller, C.R. Wagner, Measuring Discharge with Acoustic Doppler Current Profilers from a Moving Boat, USGS, 2009, p. 72.
[34] K. Gunn, C. Stock-Williams, On validating numerical hydrodynamic models of complex tidal flow, Int. J. Marine. Energy 3—4 (2013) e82—e97.
[35] McCann, D.L. and P.S. Bell. Marine radar derived current vector mapping at a planned commercial tidal stream turbine array in the Pentland Firth, UK. in Oceans 2014. St Johns, Canada: IEEE.
[36] P.S. Bell, J. Lawrence, J.V. Norris, Determining currents from marine radar data in an extreme current environment at a tidal energy test site, in: 2012 IEEE International Geoscience and Remote Sensing Symposium, IEEE, 2012, pp. 7647—7650.
[37] L. Mackie, P.S. Evans, M.J. Harrold, T. O'Doherty, M.D. Piggott, A. Angeloudis, Modelling an energetic tidal strait: investigating implications of common numerical configuration choices, Appl. Ocean Res. 108 (2021).
[38] L. Wyatt, Wave and tidal power measurement using HF radar, Int. Marine. Energy. J. 1 (2018).
[39] T. Harrison, K.M. Thyng, B. Polagye, Comparative evaluation of volumetric current measurements in a tidally dominated coastal setting: a virtual field experiment, J. Atmos. Ocean. Technol. 37 (4) (2020) 533—552.
[40] J. McIlvenny, B.J. Williamson, C. MacDowall, P. Gleizon, R. O'Hara Murray, Modelling hydrodynamics of fast tidal stream around a promontory headland, Estuar. Coast Shelf Sci. 259 (2021), 107474.
[41] V. Klemas, Remote sensing of coastal and Ocean currents: an overview, J. Coast Res. 28 (3) (2012) 576—586.
[42] K. Dohan, Ocean surface currents from satellite data, J. Geophys. Res. C Oceans 122 (4) (2017) 2647—2651.
[43] I. Fujita, M. Muste, A. Kruger, Large-scale particle image velocimetry for flow analysis in hydraulic engineering applications, J. Hydraul. Res. 36 (3) (1998) 397—414.
[44] A. Hauet, J.D. Creutin, P. Belleudy, M. Muste, W. Krajewski, Discharge measurement using Large Scale PIV under varied flow conditions - recent results, accuracy and perspectives, in: International Conference on Fluvial Hydraulics, Lisbon, PORTUGAL, 2006.
[45] F. Tauro, A. Petroselli, E. Arcangeletti, Assessment of drone-based surface flow observations, Hydrol. Process. 30 (7) (2016) 1114—1130.
[46] C. Pagano, F. Tauro, S. Grimaldi, M. Porfiri, Development and testing of an unmanned aerial vehicle for large scale particle image velocimetry, in: ASME 2014 Dynamic Systems and Control Conference, 2014.
[47] R.A. Holman, K.L. Brodie, N.J. Spore, Surf zone characterization using a small quadcopter: technical issues and procedures, IEEE Trans. Geosci. Rem. Sens. 55 (4) (2017) 2017—2027.
[48] D. Perkovic, T.C. Lippmann, S.J. Frasier, Longshore surface currents measured by Doppler radar and video PIV techniques, IEEE Trans. Geosci. Rem. Sens. 47 (8) (2009) 2787—2800.
[49] J.A. Puleo, G. Farquharson, S.J. Frasier, K.T. Holland, Comparison of optical and radar measurements of surf and swash zone velocity fields, J. Geophys. Res. C Oceans 108 (C3) (2003).
[50] I. Rodríguez-Padilla, B. Castelle, V. Marieu, P. Bonneton, A. Mouragues, K. Martins, D. Morichon, Wave-filtered surf zone circulation under high-energy waves derived from video-based optical systems, Rem. Sens. 13 (10) (2021) 1874.
[51] P. Dérian, R. Almar, Wavelet-based optical flow estimation of instant surface currents from shore-based and UAV videos, IEEE Trans. Geosci. Rem. Sens. 55 (10) (2017) 5790—5797.
[52] J. Dawoon, L. Jong-Seok, B. Ji-Yeon, N. Jungho, J. Young-Heon, S. Kyu-Min, C. Yoeng Il, High temporal and spatial resolutions of sea surface current from

low-altitude remote sensing, J. Coast Res. 90 (sp1) (2019) 282—288.

[53] N. Rüssmeier, A. Hahn, O. Zielinski, Ocean surface water currents by large-scale particle image velocimetry technique, in: OCEANS 2017 - Aberdeen, 2017.

[54] L. Lieber, R. Langrock, W. Nimmo-Smith, A Bird's-Eye View on Turbulence: Seabird Foraging Associations with Evolving Surface Flow Features, Proceedings of the Royal Society B: Biological Sciences, 2021, p. 288.

[55] L. Lieber, W.A.M. Nimmo-Smith, J.J. Waggitt, L. Kregting, Localised anthropogenic wake generates a predictable foraging hotspot for top predators, Commun.Biol. 2 (1) (2019) 123.

[56] J. Slingsby, B.E. Scott, L. Kregting, J. McIlvenny, J. Wilson, A. Couto, D. Roos, M. Yanez, B.J. Williamson, Surface characterisation of kolk-boils within tidal stream environments using UAV imagery, J. Mar. Sci. Eng. 9 (5) (2021).

[57] M. Raffel, C.E. Willert, F. Scarano, C. Kähler, S.T. Wereley, J. Kompenhans, Particle Image Velocimetry: A Practical Guide, 3 ed., vol. 669, Springer International Publishing, 2018.

[58] Q.W. Lewis, B.L. Rhoads, Resolving two-dimensional flow structure in rivers using large-scale particle image velocimetry: an example from a stream confluence, Water Resour. Res. 51 (10) (2015) 7977—7994.

[59] J.P. Leitão, S. Peña-Haro, B. Lüthi, A. Scheidegger, M. Moy de Vitry, Urban overland runoff velocity measurement with consumer-grade surveillance cameras and surface structure image velocimetry, J. Hydrol. 565 (2018) 791—804.

[60] W. Thielicke, E.J. Stamhuis, PIVlab — towards user-friendly, affordable and accurate digital particle image velocimetry in MATLAB, J. Open Res. Software 2 (1) (2014) 30.

[61] W. Thielicke, R. Sonntag, Particle image velocimetry for MATLAB: accuracy and enhanced algorithms in PIVlab, J. Open Res. Software 9 (1) (2021) 12.

[62] H. Ben-Gida, R. Gurka, A. Liberzon, OpenPIV-MATLAB - an Open-Source Software for Particle Image Velocimetry; Test Case: Birds' Aerodynamics vol. 12, Softwarex, 2020.

[63] D. Sivas, A.B. Olcay, H. Ahn, Investigation of a corrugated channel flow with an open source PIV software, in: 10th Anniversary International Conference on Experimental Fluid Mechanics, 2015. Prague, CZECH REPUBLIC.

[64] J. Le Coz, M. Jodeau, A. Hauet, B. Marchand, R. Le Boursicaud, Image-based velocity and discharge measurements in field and laboratory river engineering studies using the free FUDAA-LSPIV software, in: River Flow, Lausanne, Switzerland, 2014.

[65] S. Pearce, R. Ljubičić, S. Peña-Haro, M. Perks, F. Tauro, A. Pizarro, S.F. Dal Sasso, D. Strelnikova, S. Grimaldi, I. Maddock, G. Paulus, J. Plavšić, D. Prodanović, S. Manfreda, An evaluation of image velocimetry techniques under low flow conditions and high seeding densities using unmanned aerial systems, Rem. Sens. 12 (2) (2020).

[66] W.-C. Liu, C.-H. Lu, W.-C. Huang, Large-scale particle image velocimetry to measure streamflow from videos recorded from unmanned aerial vehicle and fixed imaging system, Rem. Sens. 13 (14) (2021) 2661.

[67] X. Zhu, G. Lipeme Kouyi, An analysis of LSPIV-based surface velocity measurement techniques for stormwater detention basin management, Water Resour. Res. 55 (2) (2019) 888—903.

[68] Q.W. Lewis, E.M. Lindroth, B.L. Rhoads, Integrating unmanned aerial systems and LSPIV for rapid, cost-effective stream gauging, J. Hydrol. 560 (2018) 230—246.

[69] Q.W. Lewis, B.L. Rhoads, LSPIV measurements of two-dimensional flow structure in streams using small unmanned aerial systems: 1. Accuracy assessment based on comparison with stationary camera platforms and in-stream velocity measurements, Water Resour. Res. 54 (10) (2018) 8000—8018.

[70] F. Tauro, R. Piscopia, S. Grimaldi, Streamflow observations from cameras: large-scale particle image velocimetry or particle tracking velocimetry? Water Resour. Res. 53 (12) (2017) 10374—10394.

[71] S. Creëlle, R. Roldan, A. Herremans, D. Meire, K. Buis, P. Meire, T. Van Oyen, T. De Mulder, P. Troch, Validation of large-scale particle image velocimetry to acquire free-surface flow fields in vegetated rivers, J. Appl. Water. Eng. Res. 6 (3) (2018) 171—182.

[72] P. Koutalakis, O. Tzoraki, G. Zaimes, UAVs for hydrologic scopes: application of a low-cost UAV to estimate surface water velocity by using three different image-based methods, Drones 3 (1) (2019) 14.

[73] M. Lewis, S.P. Neill, P.E. Robins, M.R. Hashemi, Resource assessment for future generations of tidal-stream energy arrays, Energy 83 (2015) 403—415.

[74] OES-Environmental. Ramsey Sound, 2017 [cited 2021 29/11/2021]; Available from: https://tethys.pnnl.gov/project-sites/ramsey-sound.

[75] Ltd, C.O.S.W. [cited 2021 29/11/2021]; Available from: https://cambrian-offshore.com/.

[76] P. Evans, A. Mason-Jones, C. Wilson, C. Wooldridge, T. O'Doherty, D. O'Doherty, Constraints on extractable power from energetic tidal straits, Renew. Energy 81 (2015) 707—722.

[77] D. Haverson, J. Bacon, H.C.M. Smith, V. Venugopal, Q. Xiao, Cumulative impact assessment of tidal stream energy extraction in the Irish Sea, Ocean Eng. 137 (2017) 417—428.

[78] D. Haverson, J. Bacon, H.C.M. Smith, V. Venugopal, Q. Xiao, Modelling the hydrodynamic and morphological impacts of a tidal stream development in Ramsey Sound, Renew. Energy 126 (2018) 876—887.

[79] Marine Themes Digital Elevation Model 1 Arc Second [ASC Geospatial Data], OceanWise, 2020. Scale 1:50000, Tiles: 5051510055.

[80] Atlantis, S. Meygen Tidal Energy Project. [cited 2021 29/11/2021]; Available from: https://simecatlantis.com/projects/meygen/..

[81] S. Draper, T.A.A. Adcock, A.G.L. Borthwick, G.T. Houlsby, Estimate of the tidal stream power resource of the Pentland Firth, Renew. Energy 63 (2014) 650—657.

[82] M.C. Easton, D.K. Woolf, P.A. Bowyer, The dynamics of an energetic tidal channel, the Pentland Firth, Scotland, Continent. Shelf Res. 48 (2012) 50—60.

[83] R.O. Murray, A. Gallego, A modelling study of the tidal stream resource of the Pentland Firth, Scotland, Renew. Energy 102 (2017) 326—340.

[84] M. Streßer, R. Carrasco, J. Horstmann, Video-based estimation of surface currents using a low-cost quadcopter, Geosci. Rem. Sens. Lett. IEEE 14 (11) (2017) 2027—2031.

[85] S.-H. Lee, J.-Y. Lee, J.-S. Choi, Lens distortion correction using a checkerboard pattern, in: Proceedings of the 7th ACM SIGGRAPH International Conference on Virtual-Reality Continuum and its Applications in Industry, Association for Computing Machinery, Singapore, 2008, p. 44.

[86] R.E. Davis, Drifter observations of coastal surface currents during CODE: the method and descriptive view, J. Geophys. Res.: Oceans 90 (C3) (1985) 4741—4755.

[87] M. Schaefer, T. Woodyer, Assessing absolute and relative accuracy of recreation-grade and mobile phone GNSS devices: a method for informing device choice, Area 47 (2) (2015) 185—196.

[88] T.H. Witte, A.M. Wilson, Accuracy of WAAS-enabled GPS for the determination of position and speed over ground, J. Biomech. 38 (8) (2005) 1717—1722.

[89] T.H. Witte, A.M. Wilson, Accuracy of non-differential GPS for the determination of speed over ground, J. Biomech. 37 (12) (2004) 1891—1898.

[90] A.D. Townshend, C.J. Worringham, I.B. Stewart, Assessment of speed and position during human locomotion using nondifferential GPS, Med. Sci. Sports Exerc. 40 (1) (2008) 124—132.

[91] I. Fairley, B. Williamson, J. McIlvenny, M. Lewis, S. Neill, I. Masters, A.J. Williams, D.E. Reeve, A preliminary assessment of the use of drones to quantify current velocities at tidal stream sites, in: European Wave and Tidal Energy Conference 2021, 2021. Plymouth.

[92] K. Zuiderveld, in: P. Heckbert (Ed.), Contrast Limited Adaptive Histogram Equalisation. Graphics Gems IV, Academic Press Professional, San Diego, 1994.

[93] M. Lewis, R. O'Hara Murray, S. Fredriksson, J. Maskell, A. de Fockert, S.P. Neill, P.E. Robins, A standardised tidal-stream power curve, optimised for the global resource, Renew. Energy 170 (2021) 1308—1323.

[94] M. Lewis, S.P. Neill, P. Robins, M.R. Hashemi, S. Ward, Characteristics of the velocity profile at tidal-stream energy sites, Renew. Energy 114 (2017) 258—272.

[95] F. Tauro, C. Pagano, P. Phamduy, S. Grimaldi, M. Porfiri, Large-scale particle image velocimetry from an unmanned aerial vehicle, IEEE ASME Trans. Mechatron. 20 (6) (2015) 3269—3275.

[96] D. Strelnikova, G. Paulus, S. Kafer, K.H. Anders, P. Mayr, H. Mader, U. Scherling, R. Schneeberger, Drone-based optical measurements of heterogeneous surface velocity fields around fish passages at hydropower dams, Rem. Sens. 12 (3) (2020).

[97] J. Slingsby, B. Scott, L. Kregting, J. McIlvenny, J. Wilson, M. Yanez, S. Langlois, B.J. Williamson, Using unmanned aerial vehicle (UAV) imagery to characterise pursuit-diving seabird association with tidal stream hydrodynamic habitat features, Front. Mar. Sci. (2022), https://doi.org/10.3389/fmars.2022.820722.

[98] R. Almar, E.W.J. Bergsma, P.A. Catalan, R. Cienfuegos, L. Suarez, F. Lucero, A. Nicolae Lerma, F. Desmazes, E. Perugini, M.L. Palmsten, C. Chickadel, Sea state from single optical images: a methodology to derive wind-generated ocean waves from cameras, drones and satellites, Rem. Sens. 13 (4) (2021) 679.